Assessment of organic Rankine cycle configurations for solar polygeneration orientated to electricity production and desalination

Hadrien Jaubert, Philippe Borel, Pierrette Guichardon, Jean-François Portha, Jean-Noël Jaubert, Lucie Coniglio

Assessment of organic Rankine cycle configurations for solar polygeneration orientated to electricity production and desalination

Hadrien Jaubert [a,b], Philippe Borel [a], Pierrette Guichardon [b], Jean-François Portha [c], Jean-Noël Jaubert [c], Lucie Coniglio [c,*]

[a] Université de Lorraine - Lycée Henri Poincaré, 2 Rue de la Visitation, 54000 Nancy, France
[b] Aix Marseille Université, CNRS, Centrale Marseille, M2P2 UMR 7340, Pôle de l'Étoile, Technopôle de Château-Gombert, 38 rue Frédéric Joliot-Curie, 13451 Marseille, France
[c] Université de Lorraine - Ecole Nationale Supérieure des Industries Chimiques de Nancy, Laboratoire Réactions et Génie des Procédés (UMR CNRS 7274), 1 rue Grandville, 54000 Nancy Cedex, France

ARTICLE INFO

Keywords:
Organic Ranking cycle
Working fluids
Solar polygeneration
Desalination
Reverse osmosis
Low-temperature multi-effect distillation

ABSTRACT

This work addresses the polygeneration concept integrating concentrating solar power (CSP) with an organic Rankine cycle (ORC) to produce electricity and drinking water by hybrid desalination process combining reverse osmosis (RO) and low-temperature multi-effect distillation (LTMED). Experiments carried out on a bench scale RO pilot led to determine optimal operating parameters as well as options to mitigate the main limiting factors of this technology by hybridizing with LTMED. These data helped to simulate a large scale solar polygeneration plant integrating parabolic trough collectors as CSP technology and a hybrid RO-LTMED system as desalination technology. Various ORC design proposals were simulated and the optimal configuration was pointed out on the basis of thermodynamic criteria (energy efficiency and exergy destruction) and an economic analysis by using two working fluids: an alkane commonly admitted as good candidate and an ester proposed here as green alternative. Results obtained in this work contribute positively to extending the solar polygeneration for desalination and production of energy leading to future sustainable plants.

1. Introduction

Faced with growing energy needs and imminent water stress due to global warming, accentuated itself by an increase in anthropogenic greenhouse gas emissions [1], appropriate solutions for sustainable development are essential.

An alternative is the polygeneration concept which being based on process intensification makes possible to simultaneously obtain several products, chemical or energetic, from a single source of energy, preferably renewable [2,3]. Particularly, by combining smartly the polygeneration concept with solar energy, it is possible to produce electricity and drinking water by desalination without emitting greenhouse gases [3]. The advantages of this alternative would be all the more important since more than 70% of the world lives within 70 km of coastal areas [4] and that remote areas with access to brackish water could also benefit from it.

The main features of a large-scale solar polygeneration plant for electricity production and desalination such as targeted in this work are summarized in Table 1 [2,3,5–23]. The solar technology commonly used to drive large-scale polygeneration plants with integrated desalination is the concentrating solar power (CSP) technology of which parabolic trough collectors (PTCs) are the most mature and effective systems according to energy, exergy and financial criteria [2,3,5,6]; particularly since they have incorporated thermal energy storage (TES) [7,8]. Associated with a thermodynamic cycle, generally an organic Rankine cycle (ORC), the PTCs play there the heat source required to vaporize the

Abbreviations: CAPEX, Capital expenditures; CSP, Concentrating solar power; EB, Ethyl butanoate; EoS, Equation of state; ERD, Energy recovery device; HTF, Heat transfer fluid; IP, Isopentane, also designated R601a in the refrigerant list by IUPAC; LTMED, Low-temperature multi-effect distillation; ORC, Organic Rankine cycle; PTC, Parabolic trough collector; PV, Photovoltaic; PWT, Pelton wheel turbine; RO, Reverse osmosis; RC, Rankine cycle; RR, Recovery ratio; SW, Seawater; TES, Thermal energy storage; VP, Vaporized mole fraction; ZLD, Zero-liquid-discharge.

* Corresponding author.
E-mail addresses: hadrien.jaubert@centrale-marseille.fr (H. Jaubert), phiborel54@gmail.com (P. Borel), pierrette.guichardon@centrale-marseille.fr (P. Guichardon), jean-francois.portha@univ-lorraine.fr (J.-F. Portha), jean-noel.jaubert@univ-lorraine.fr (J.-N. Jaubert), lucie.coniglio@univ-lorraine.fr (L. Coniglio).

Nomenclature

A^*	Intrinsic membrane permeability to pure water
C_F	Molar concentration of the saline water feed
C_k	Purchased cost of equipment k
$\dot{E}x_d$	Exergy destruction rate occurring inside the considered system
$\overline{E}x_k$	Mass exergy of the fluid flowing in stream k
$f_{g,k}$	Installation factor of equipment k
$f_{m,k}$	Material factor of equipment k
$f_{p,k}$	Factor depending on the level of pressure in equipment k
$\overline{H}_k$	Mass enthalpy of the fluid flowing in stream k
$\dot{m}_k$	Mass flowrate of the fluid flowing in stream k
$\dot{Q}_k$	Thermal power provided to or generated by unit k
$\dot{W}_k$	Mechanical power provided to or generated by unit k
P_F	Pressure of the RO module feed
P_P	Pressure of the permeate outgoing the RO module
P_R	Pressure of the retentate outgoing the RO module
Q_P	Permeate volume flowrate
R	Ideal gas constant
R_m	Intrinsic membrane resistance
R_s	Resistance of the retained salts
S_f	Membrane filtering surface
$\overline{S}_k$	Mass entropy of the fluid flowing in stream k
T_F	Temperature of the saline water feed
T_k	Temperature of the fluid flowing in stream k
T_{ref}	Reference temperature (293.15 K)
TMP	Transmembrane pressure
$\Delta\pi$	Osmotic pressure difference between the membrane-liquid interfaces
η	Turbine or pump isentropic efficiency
η_{ORC}	Thermal efficiency of the ORC
μ	Liquid water viscosity
π_F	Osmotic pressure of the feed saline water

working fluid flowing through the cycle. After this stage of vaporization, the fluid is expanded in a turbine to generate the desired mechanical power (that can be converted in electricity thanks to an alternator), and then is fully condensed through a cold source, to be finally pumped to the PTCs, closing thus the cycle. Regarding large-scale desalination processes, the two main routes sharing respectively 70 and 25% of the market are: the membrane route by reverse osmosis (RO) and the thermal route by low-temperature multiple-effect distillation (LTMED) [15,18,24]. For RO desalination, a fraction of the mechanical power delivered by the ORC is used to run the process high-pressure pump [13,14] while for LTMED desalination, the first effect stands for the ORC cold source [18,19]. With regards to seawater, the energy consumption and water production costs of the RO process are lower than for the LTMED process, particularly over the recent years due to the material and technological developments in RO desalination [16]. Nonetheless, the RO technology requires more intensive pretreatment for extension of the membrane lifetime with chemical additives having impacts on aquatic life [15]. From a techno-economic analysis, **Palenzuela et al.** [25,26] also concluded that the coupling PTC-LTMED was more suitable than the coupling PTC-RO, both thermodynamically and economically. However, **Palenzuela et al.** [27] emphasized more recently that on the basis of annual production of electricity and fresh water (that includes transient operating of the solar desalination plant), CSP system led to maximum production when combined with RO rather with LTMED. Furthermore, a recent study carried out in Venezuela and northern Chile demonstrated that a polygeneration plant incorporating PTCs and LTMED could provide electricity and fresh water to more than 85,000 inhabitants at a reasonable cost (170 USD/MWh and 1.4 USD/m^3) [7]. The authors also highlighted that plant feasibility and costs highly depend on the specific conditions of each country (mainly the water and energy stress levels, the irradiation, the proximity and salinity rate of water), which was reinforced very recently by other authors [16]. Other recent studies also pointed out the ORC configuration [3,6,28] and the selected working fluid [3,28,29] as other key levers to improve the performance of the solar polygeneration concept aiming desalination and electricity production. Particularly, **Zheng et al.** [10] emphasized the critical role of the thermal integration in the ORC for reducing exergy destruction and making thus efficient the coupling of solar collectors with desalination systems. Also, a final important aspect common to desalination technologies is the brine management for which treatment systems based on the Zero-Liquid-Discharge concept are still under development [17].

Therefore, this work addresses the modelling and simulation of a polygeneration plant integrating solar PTCs with an ORC to produce electricity and drinking water via a hybrid RO-LTMED desalination system, by working on the ORC and the brine upgrading (Table 1, [2,3,5–23]). Various ORC designs were analyzed by using two working fluids: an alkane commonly admitted as a good candidate for the focused objectives and an ester proposed here as a green alternative. Regarding the hybrid desalination scheme adopted, the brine from the RO unit was routed to the LTMED. For each investigated design, simulation of the ORC with a given working fluid was conducted and the optimal configuration was pointed out on the basis of thermodynamic criteria (maximum energy efficiency and minimum exergy destruction) followed by an economic analysis. While the key requirements of the whole plant and of the solar PTCs were taken from two case studies achieved in the literature [7,28], information required to model the RO unit were obtained from experiments carried out on a similar bench scale unit. Hence, the novelty of this work lays on both the green alternative proposed as working fluid and on the hybridization of the desalination system for upgrading the brine, in line with the zero-liquid-discharge concept.

2. Methodology

PROII software [30] was selected as process simulator. The base flow diagram modelling with PROII [30] the key units of the solar polygeneration plant considered in this work is described in Fig. 1. The Peng-Robinson equation of state [31] was used to estimate the thermophysical properties and phase-equilibria of all fluids involved in the plant, i.e. the heat transfer fluid (HTF), the working fluid, and seawater. Although performant for simulating thermodynamic behavior of systems involving non-associated organic molecules within a large range of temperature, pressure, and composition (average deviations lower than 2% for pure component properties, [32]), the Peng-Robinson equation of state (EoS) is however not appropriate for systems involving dissolved salts. Moreover, the thermodynamic consistency is no more guaranteed when simulating a plant with different thermodynamic models. Because of these reasons, seawater with a typical salinity of about 35 g/kg was assumed here to be pure water. Specific enthalpy of seawater being lower than that of pure water (while it is the reverse for the boiling temperature at given pressure) [33], this assumption leads to overestimate the heat power required to the LTMED process. Therminol VP-1 (composition in wt %: 73.5 diphenyl oxide, 26.5 diphenyl; streams SOLAR_1 and SOLAR_2 in Fig. 1) was selected as HTF for its thermal stability and suitable operation over long periods at temperatures up to 400 °C [5,28,34]. The selection of the organic working fluid is presented just after, in subsection 2.1.

Table 1
Research gaps and key issues to be addressed, objective and novelty of this work [2,3,5–23]

1-Key subsystems of a large-scale solar polygeneration plant dedicated to electricity production and desalination and the features targeted in this work			
Subsystems	Attractive features for the present work	Gaps and key issues to be addressed	Connections with this work and objective
•Solar technology			
Parabolic through collectors (PTCs) associated with a Rankine cycle operating with an organic working fluid (organic Rankine cycle, ORC)	-Capable of large-scale electric power generation [2,3,5,6] without irregularity issues thanks to incorporation of thermal energy storage (TES) with molten salts [7,8] -Options not possible with photovoltaic panel (PV) technology [9] -Possibility of combining them with membrane (reverse osmosis) or thermal (multiple-effect distillation) desalination processes, with particular benefits on large-scale [10]	-Alternatives to enhance the PTCs performance and thus to reduce their costs that remain higher than for PV panels -Complexity in the determination of the optimal alternative due to a strong interdependence between the working fluid, the working conditions and the cycle architecture; the integrated solar technology included [10,11,12] -Importance of controlling simultaneously the thermal efficiency and the exergy destruction rate of the system [10]	-Decrease of the thermal power required from the PTCs by enhancing the ORC performance through an adapted combination of the ORC design and of the working fluid, on the basis of thermodynamic criteria (maximum energy efficiency and minimum exergy destruction) followed by an economic analysis
•Desalination technology			
Reverse osmosis (RO)	-Requirement of an external mechanical power to run the RO high-pressure pump which is needed to counter the osmotic pressure imposed by the difference in salts concentration on either side of the membrane leading to the permeate (drinking water) and the brine (byproduct with high salinity) [13,14] -Low operating temperature [13,14] -Energy consumption and water production costs lower than for the LTMED technology [15], especially over the recent years due to the material and technological developments in RO desalination [16]	-Need of intensive pretreatment for extension of the membrane lifetime with chemical additives having impacts on aquatic life [15,16] -Brine management; indeed, the brine which is the byproduct of the desalination processes has negative impact for environment due to its high salinity [16,17].	-The mechanical power delivered by the ORC is partly extracted for running the high-pressure pump of the RO process. -Seawater is used to play partly the ORC cold source for enhancing the desalination performance of the RO process.
Low-temperature multiple-effect distillation (LTMED)	-Requirement of an external thermal energy to cause evaporation of the saline water in the first effect. This external thermal energy is however the only one to provide since the vapors thus formed are used to heat the successive effects and then are condensed to yield the pure water distillate while the brine accumulates at the bottom and flows out to the last effect [18,19]. -Operating under low temperature reduces fouling issues [7] -Could be appropriate for brine treatment after material upgrade to prevent corrosion issues [17]	-External thermal energy supplied conventionally by fossil fuel combustion and more occasionally by solar energy [10,18] -Requirement of mineral addition into the distillate to make it drinkable -Brine management; indeed, the brine which is the byproduct of the desalination processes has negative impact for environment due to its high salinity [16,17].	-The first effect of the LTMED process stands for the ORC cold source where the vapor state working fluid (flowing inside the tube bundle) is condensed and the saline water (sprayed outside the tube bundle) is partly vaporized [18,19].
2-Novelty of this work			
-Selection of a green alternative as working fluid: ethyl butanoate -Hybridization of RO and LTMED technologies by using RO for seawater desalination and LTMED for concentrating part of the RO brine, in line with the Zero-Liquid-Discharge concept [17] -Ultimately rejected brine fate: solar ponds or sodium-ion batteries, regarding the concentrated brine from the LTMED process [15,20,21] or aquaculture/thalassotherapy, regarding the brine from the RO process [18]; for both brine types: electrodialysis with bipolar membranes to produce acids (HCl) and bases (NaOH) by using eventually nanocomposite anion exchange membranes to improve the RO desalination stability [22,23].			

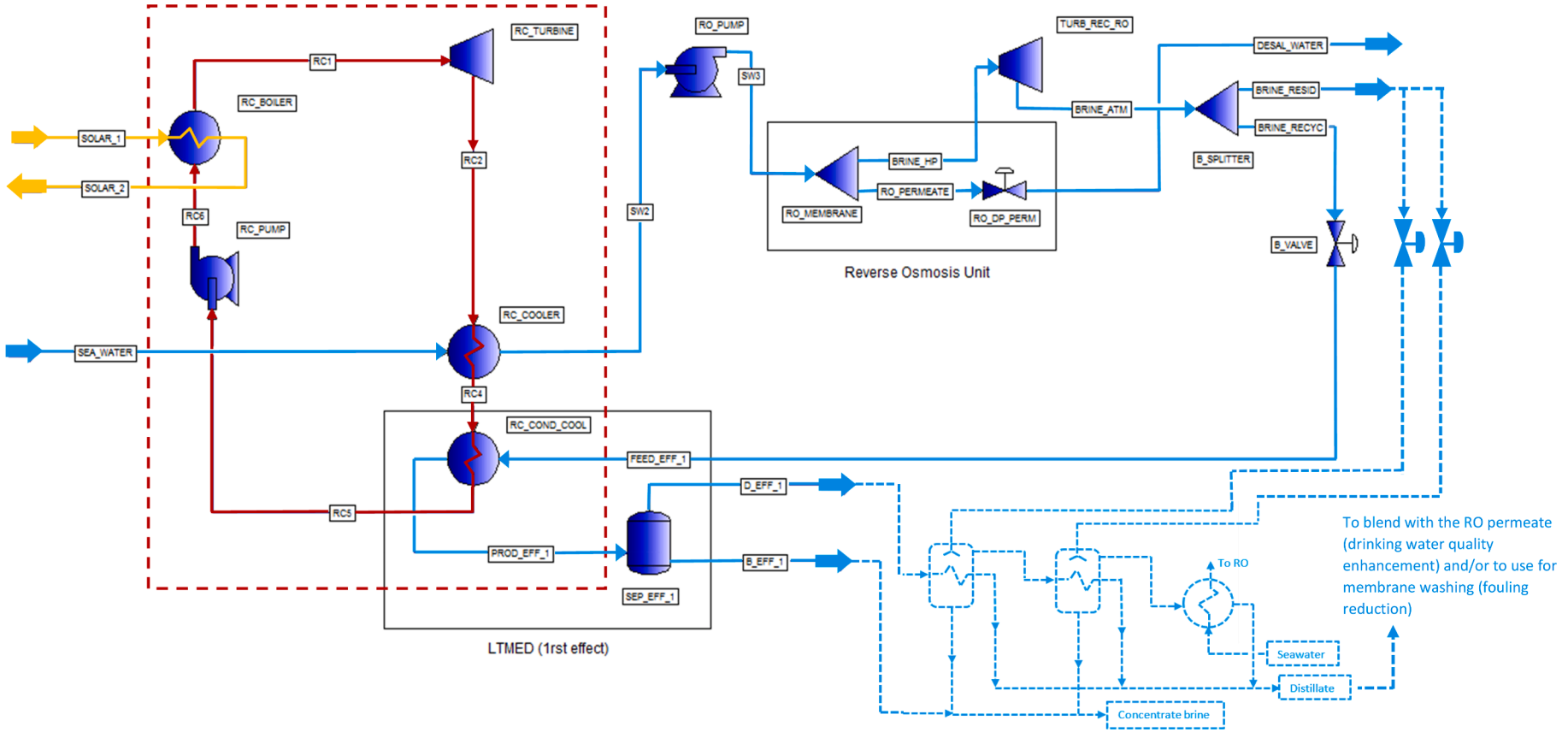

Fig. 1. Modelling with ProII of the investigated solar polygeneration plant dedicated to electricity production and desalination by hybrid RO-LTMED system – Base ORC (configuration 1). ——: heat transfer fluid; ——: working fluid; - - - - -: ORC boundary; ——: seawater.

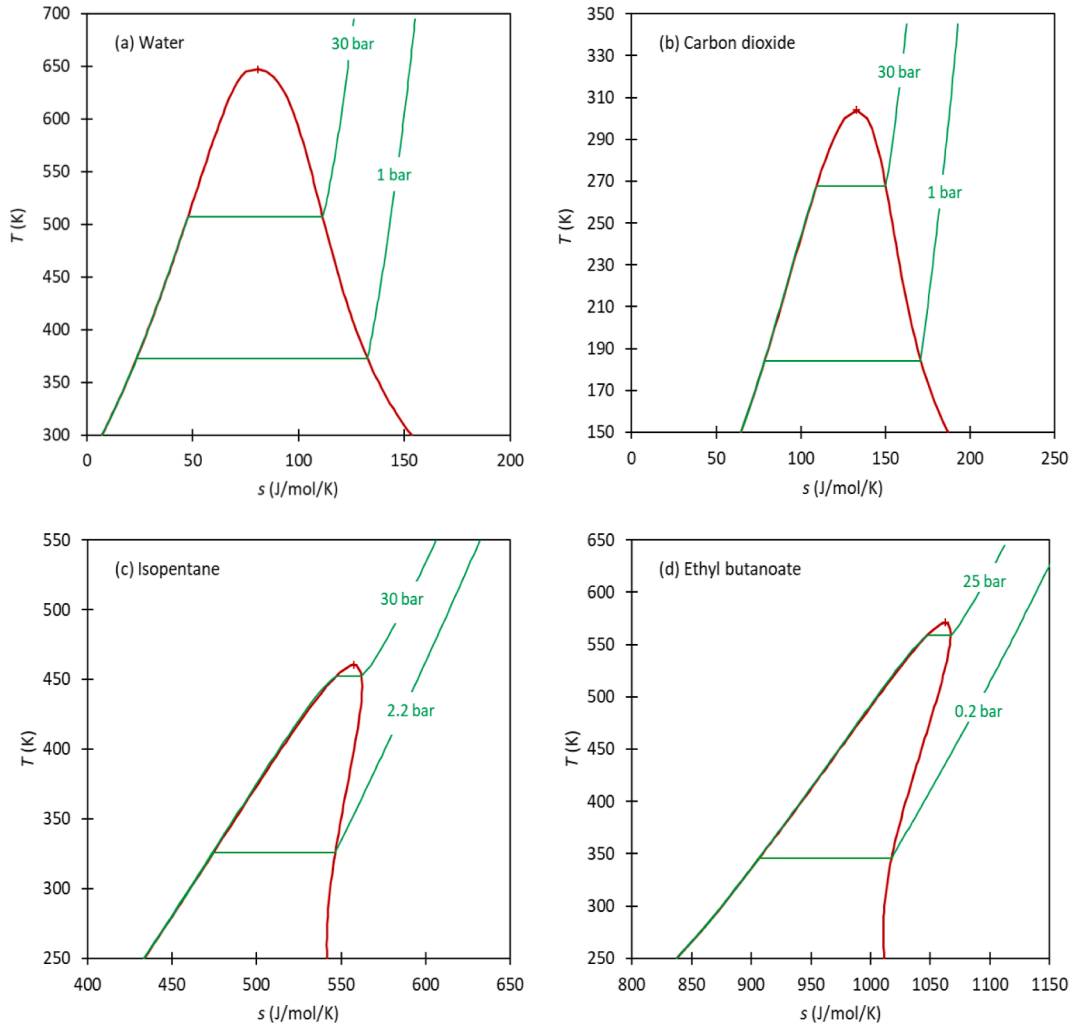

Fig. 2. *T-s* diagrams for common and potential working fluids calculated with Peng-Robinson EoS [31,32]. The saturation curve separating the two vapor–liquid phase region from the one phase region is plotted in red while isobars delimiting the Rankine cycle pressure range are plotted in green. Reference for enthalpies: saturated liquid at 273.15 K for water, 271.80 K for carbon dioxide, 270.92 K for isopentane, and 256.56 K for ethyl butanoate; reference for entropies: saturated liquid at 273.15 K for water; liquid at 58.98 K for carbon dioxide, 13.15 K for isopentane, 10.44 K for ethyl butanoate.

2.1. Working fluids selected

The working fluid selection is an essential step for an efficient Rankine cycle modelling. Indeed, if considering a turbine inlet at saturated vapor state, the working fluid under high pressure has to remain vapor all along its expansion through the turbine in order to avoid blade erosion by liquid droplet formation. Thus, such a condition implies that the slope of the vapor side saturation curve in the temperature-entropy (*T-s*) diagram be positive or at least infinite; the working fluids being thus referred to as respectively dry or isentropic (wet if the slope is negative) [11,35]. Fig. 2 depicts the *T-s* diagrams of working fluids typically used in Rankine cycles depending their operating conditions, i.e. under high (**a**), low (**b**) or medium (**c**) temperatures. As it can be observed, water and carbon dioxide (i.e. wet working fluids) require first to be superheated not to cross the two-phase domain after isentropic expansion, unlike the two other dry fluids depicted by Fig. 2, i.e. isopentane (**c**) and ethyl butanoate (**d**).

Despite the criterion mentioned above, no single working fluid has been identified as optimal for a given ORC. This is mainly due to the strong interdependence between the working fluid, the working conditions, and the cycle architecture; the integrated CSP system included [11,12]. A computer-based method integrating process and working fluid design for ORCs was recently proposed [29]. Constructed from the SAFT-γ-Mie EoS using the group contribution approach [36], the top 10 candidates are mainly alkanes and alkenes with several ethers, but none of them contains ester, alcohol, or carboxylic acid functional groups, suggesting that these chemical families are unfavorable. Nonetheless, thermodynamic models based on the group contribution approach may estimate physical properties and phase equilibria with some uncertainty. Furthermore, the authors [29] mentioned that, for the ORC configurations considered in their work, the same list of candidates was obtained but with different rankings.

As a result, isopentane (IP) that was recommended as one of the best working fluid candidates for solar ORCs in various studies [11,28,37] was selected in this work, together with ethyl butanoate (EB) as green alternative. Indeed, in addition to being a dry fluid (Fig. 2d), preliminary simulations of ORCs with EB as working fluid have revealed promising performance.

2.2. Base organic Rankine cycle

As a turbine delivers a high mechanical power when high pressure ratio is applied, one might be tempted to expand higher and lower pressure limits of the ORC. Nevertheless, near the critical point of the working fluid, small changes in temperature induce large changes in pressure, which makes the ORC unstable. Furthermore, depending on

Table 2
Specifications of the PTCs, ORC, and hybrid RO-LTMED system for modelling and simulating the whole solar polygeneration plant investigated (Fig. 1).[a]

Actual unit or fluid	Modelling unit or stream (name)	Parameter	Value	
		ORC Configuration	Working fluid	
		1 / 2 / 3	EB	IP
ORC heat source (solar PTCs)	Heat exchanger (RC_BOILER)	Cold product (RC1) liquid fraction	0	
ORC turbine	Turbine (RC_TURBINE)	Outlet (RC2) pressure / Removed	0.20 bar [b]	2.20 bar [b]
		η	0.90	0.90
ORC turbine first stage	Turbine (RC_TURBINE_1)	Not included / Outlet (RC2.1) pressure	2.24 bar	8.12 bar
		η	0.90	0.90
ORC re-heater	Heat exchanger (RC_RE_HEATER)	Not included / Cold product (RC2.2) temperature	Defined as RC1 stream temperature	
ORC turbine second stage	Turbine (RC_TURBINE_2)	Not included / Outlet (RC2) pressure	0.20 bar	2.20 bar
		η	0.90	0.90
ORC self-heat recuperation technology (regenerator)	Heat exchanger (RC_REGEN)	Not included / Hot product (RC3) liquid fraction	0	
First part of the ORC cold source	Heat exchanger (RC_COOLER-RC_CONDENS) [d]	Cold product (SW2) temperature	25°C [c]	
Second part of the ORC cold source	Heat exchanger (RC_COND_COOL)	Hot product (RC5) temperature drop below bubble point	7°C	
ORC pump	Pump (RC_PUMP)	Outlet (RC1) pressure	25 bar [e]	30 bar [e]
		η	0.80	0.80
RO pump	Pump (RO_PUMP)	Outlet (SW3) pressure	65 bar [c]	
		η	0.80	
RO process	Splitter (RO_MEMBRANE)	$\dot{m}_{RO\_PERMEATE}/\dot{m}_{SW3}$	0.50 [c]	
	Valve (RO_DP_PERM)	Outlet (DESAL_WATER) pressure	1 bar [c]	
RO energy recovery Pelton wheel turbine	Turbine (TURB_REC_RO)	Outlet (BRINE_ATM) pressure	1 bar	
		η	0.98	
Junction equipment between the RO and LTMED processes	Splitter (B_SPLITTER)	$\dot{m}_{BRINE\_RECYC}/\dot{m}_{BRINE\_ATM}$	Evaluated (see subsection 2.4)	
	Valve (B_VALVE)	Outlet (FEED_EFF_1) pressure	0.25 bar [b]	0.10 bar [b,f]
First effect of the LTMED process	Flash (SEP_EFF_1)	Pressure drop (ΔP)	0 bar	
		Duty ($\dot{Q}$)	0 MW	
Seawater	Stream (SEA_WATER)	$\dot{m}_{SEA\_WATER}$, T_{SEA_WATER}, P_{SEA_WATER}	600 kg/s, 15°C, 1 bar [g]	
HTF (Therminol VP-1)	Stream (SOLAR_1)	$\dot{m}_{SOLAR\_1}$, T_{SOLAR_1}, P_{SOLAR_1} (physical state)	1440 kg/s [h] 330°C 1 bar (vapor)	1440 kg/s [h] 220°C 1 bar (liquid)

[a]No pressure drop inside the heat exchangers.
[b]See subsection 2.4 for details.
[c]From the experiments carried out (**Appendix A** [1,13,14,28,38,39]).
[d]RC_COOLER for the ORC configuration 1, RC_CONDENS for the others.
[e]See subsection 2.2 for details.
[f]The lowest pressure accepted for the ORC condenser is 0.05 bar [11,35].
[g]From [7,28].
[h]From [28].

the *T-s* diagram shape of the working fluid, expansion starting too close to the critical point might partly cross the two-phase region. Therefore, a reasonable distance between the higher-pressure limit of the ORC and the critical point of the working fluid should be considered [11,35]. Thus, the ORC high pressure level was set to 25 or 30 bar depending on the selected working fluid, ethyl butanoate or isopentane.

Fig. 1 shows the base ORC considered in this work as departure configuration. The four key units may be observed: *(i)* the turbine (RC_TURBINE) in which the working fluid admitted at saturated vapor state is expanded from the high-pressure level to the low-pressure level; *(ii)* the condenser modelling the ORC cold source and consisting in two units, a first one (RC_COOLER) where the vapor state working fluid is precooled and a second one (RC_COND_COOL) where the working fluid still at vapor state continues to be cooled until being entirely condensed, and then sub-cooled 7 °C under its boiling temperature to secure appropriate operational conditions for the following unit; *(iii)* the pump (RC_PUMP) recycling the sub-cooled liquid working fluid from low to high pressure to *(iv)* the solar PTCs playing the ORC hot source (RC_BOILER) where the sub-cooled liquid working fluid is heated and then totally vaporized to be recycled to the saturated vapor turbine inlet. Therefore, with regard to the solar PTCs, only the preheater and the evaporator have been modeled here through the RC_BOILER. The cold-side streams of the two units modelling the ORC cold source, i.e. the RC_COOLER and RC_COND_COOL (Fig. 1), are respectively the seawater thus preheated before entering the RO pump and part of the RO brine recycled to the LTMED process for concentration and further repurposing. Further details regarding these two streams are given in the following section 2.3.

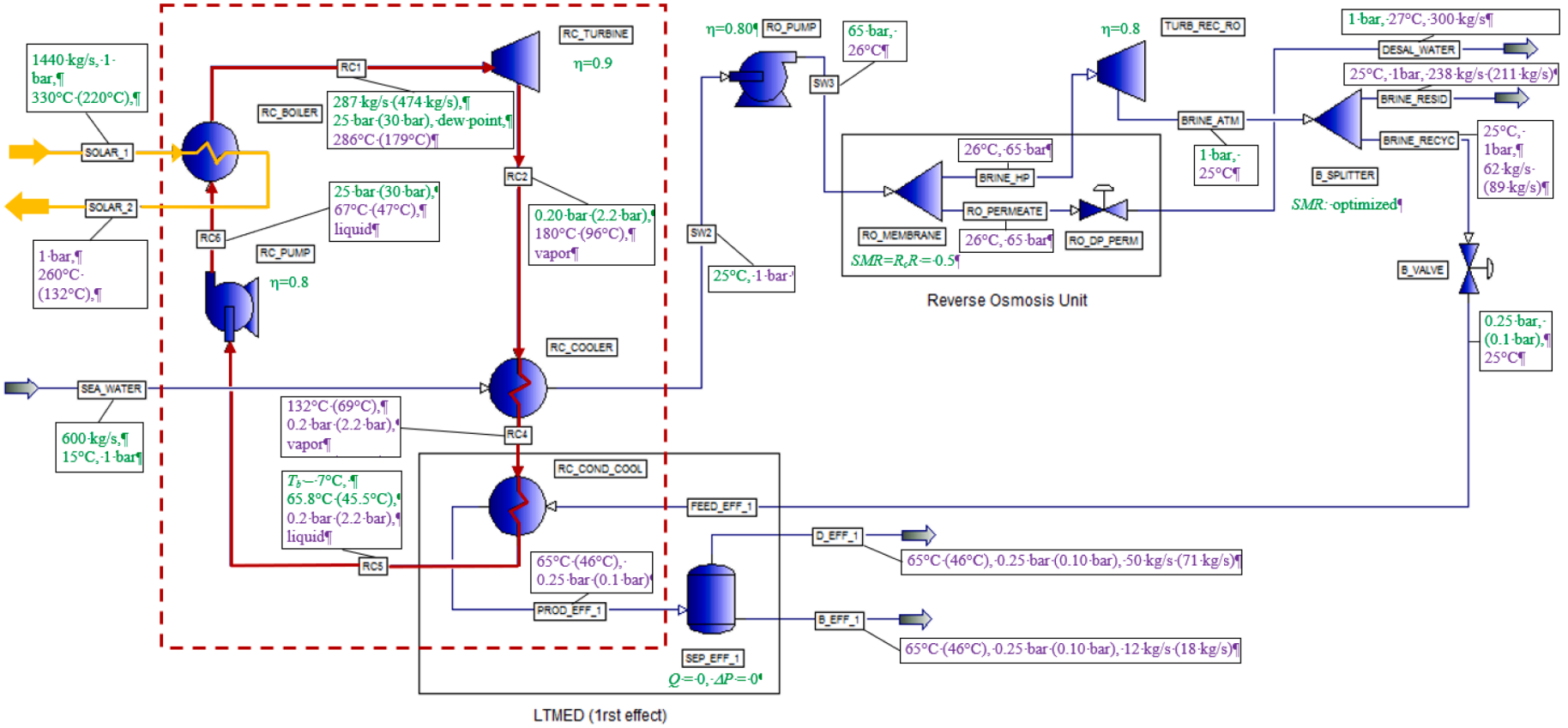

Fig. 3. Simulation results with ProII of the investigated solar polygeneration plant integrating the base ORC (configuration 1). Specifications of streams and units are written in green and results in purple, for both working fluids by using parenthesis for IP; indications are not repeated when they are the same for EB and IP. ——: heat transfer fluid; ——: working fluid; - - - -: ORC boundary; ——: seawater. *SMR*: stream molar ratio, see section 2.4 (eq. (1)) for B_SPLITTER unit. Further information is available in **Appendix C**.

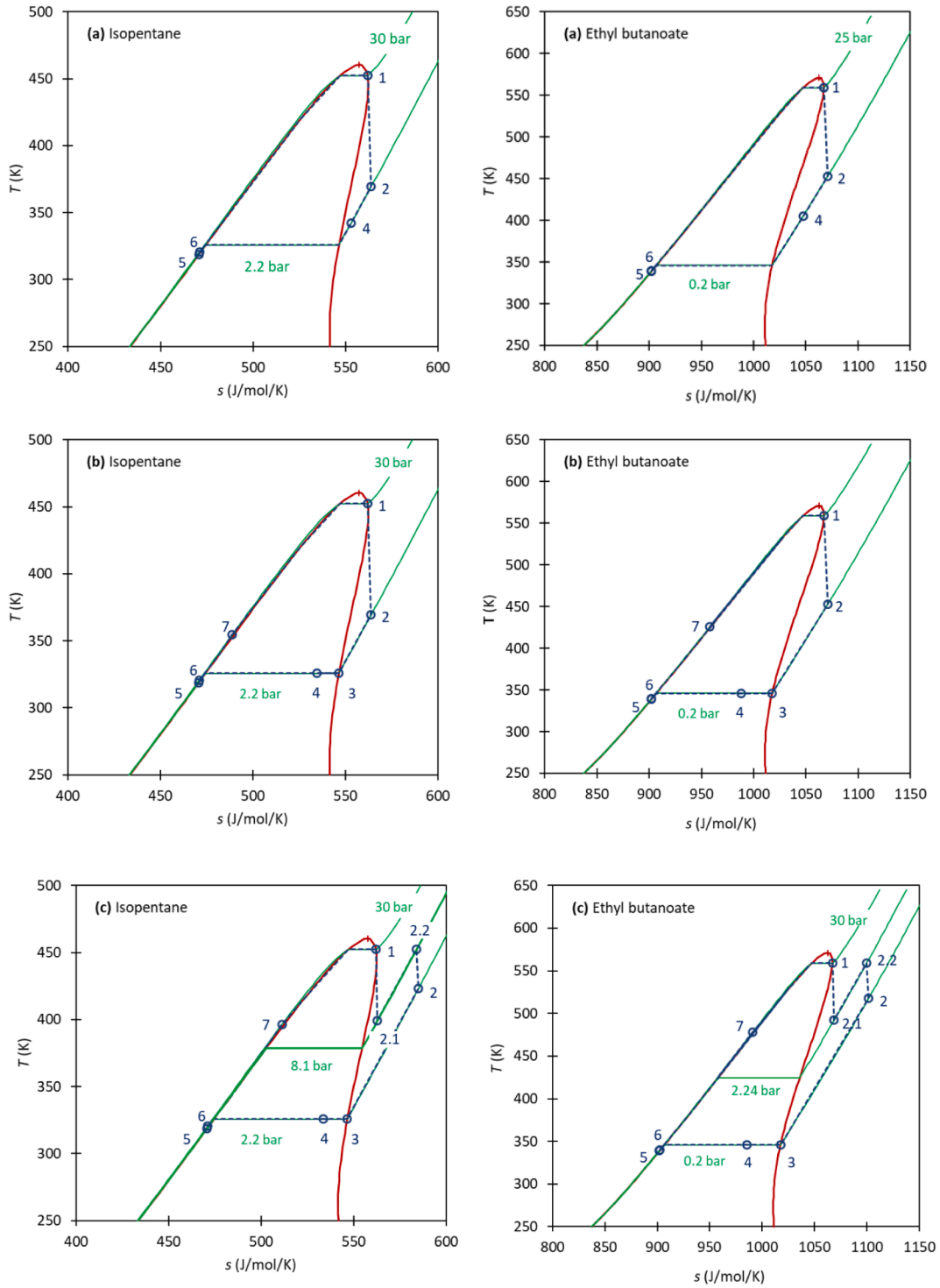

Fig. 4. *T-s* diagrams for isopentane and ethyl butanoate related to **(a)** base ORC with a single turbine and without regenerator (configuration 1); **(b)** ORC with a regenerator and a single turbine (configuration 2); **(c)** ORC with a regenerator and two turbines (configuration 3). The saturation curve separating the two vapor–liquid phase region from the one phase region is plotted in red while the isobars delimiting the ORC pressure range are plotted in green; all of them calculated with the Peng-Robinson EoS [31,32]. Reference for enthalpies: saturated liquid at 270.92 K for isopentane, and 256.56 K for ethyl butanoate; reference for entropies: liquid at 13.15 K for isopentane, 10.44 K for ethyl butanoate.

2.3. Hybrid membrane and thermal desalination system

In order to achieve the desired water quality, additional RO stages are generally required to solve the critical boron and chlorine issue which moreover implies severe operating conditions of the RO process with a shorter membrane lifetime [38]. Furthermore, decreasing performance over time is usually observed in RO processes because of concentration of polarization (salts accumulation on the membrane boundary layer) which induces fouling (salts deposit on membrane). As observed experimentally with a bench scale RO unit, this fouling phenomenon is however partly reversible and may be reduced without interrupting the unit operation by punctual pure water circulation (**Appendix A** [1,13,14,28,38,39]). Regarding the LTMED process where seawater is sprayed in the effects maintained at decreasing levels of

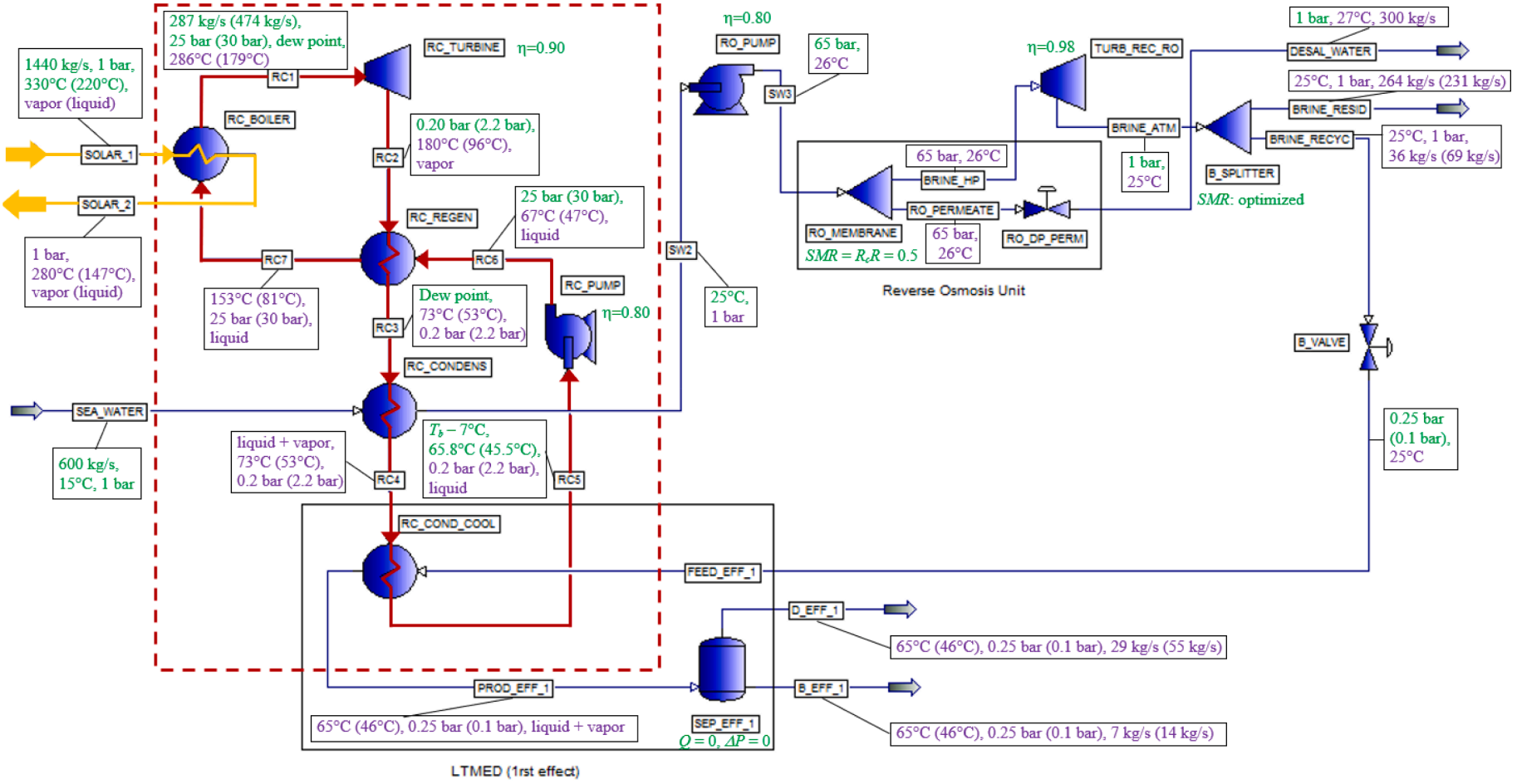

Fig. 5. Simulation results with ProII of the investigated solar polygeneration plant integrating the ORC with regenerator and single turbine (configuration 2). Specifications of streams and units are written in green and results in purple, for both working fluids by using parenthesis for IP; indications are not repeated when they are the same for EB and IP. ——: heat transfer fluid; ——: working fluid; - - - - - -: ORC boundary; ——: seawater. *SMR*: stream molar ratio, see section 2.4 (eq. (1)) for B_SPLITTER unit. Further information is available in **Appendix C**.

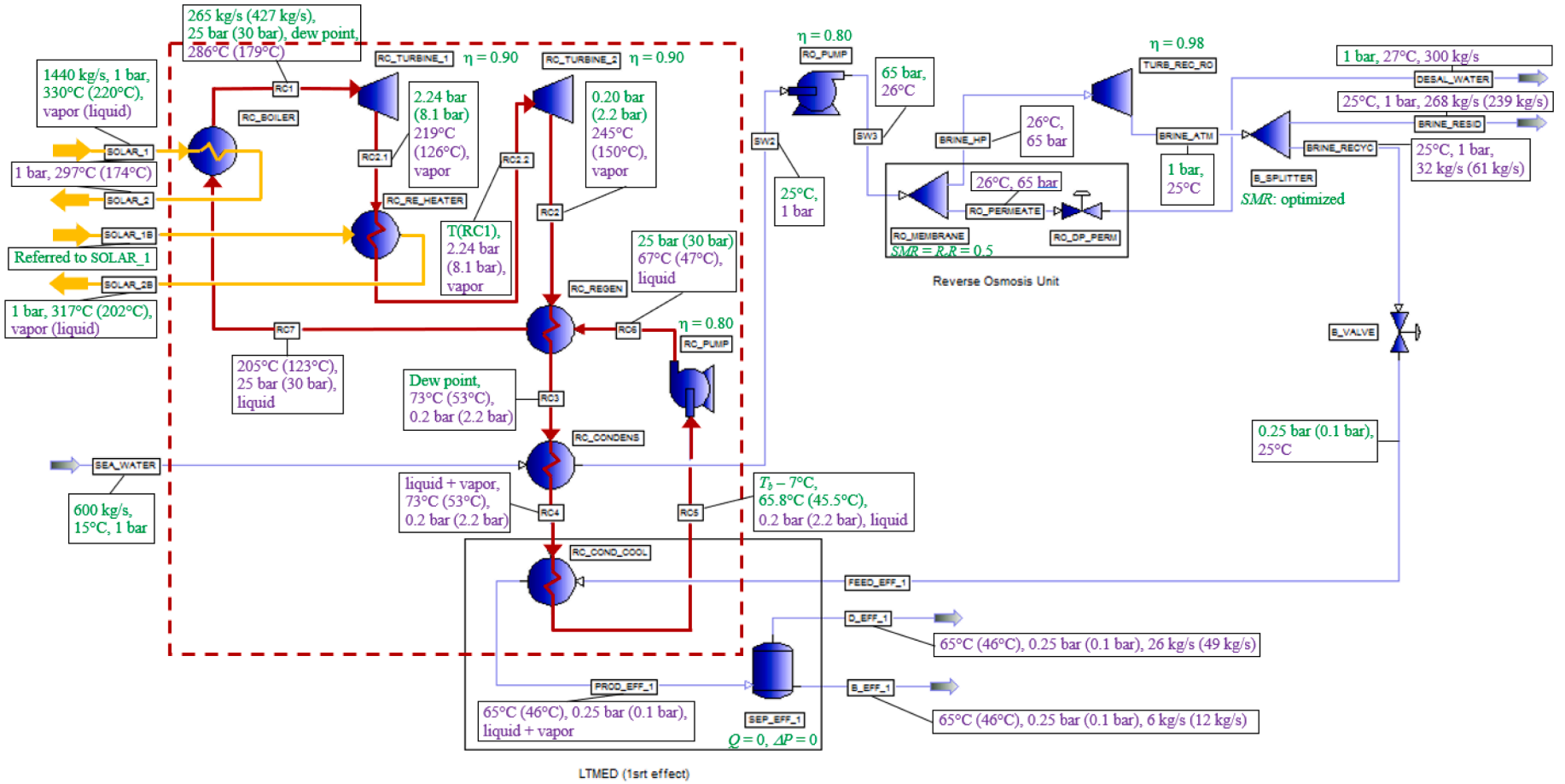

Fig. 6. Simulation results with ProII of the investigated solar polygeneration plant integrating the ORC with regenerator and two turbines (configuration 3). Specifications of streams and units are written in green and results in purple, for both working fluids by using parenthesis for IP; indications are not repeated when they are the same for EB and IP. ——: heat transfer fluid; ——: working fluid; - - - - - -: ORC boundary; ——: seawater. *SMR*: stream molar ratio, see section 2.4 (eq. (1)) for B_SPLITTER unit. Further information is available in **Appendix C**.

Table 3
Thermal analysis after simulation of the solar polygeneration plant integrating the various ORC configurations tested.

Parameter		Working fluid					
		EB			IP		
		ORC configuration			ORC configuration		
		1	2	3	1	2	3
$\dot{m}_{ORC}$(kg/s)		286.98	286.98	264.59	474.18	474.18	427.33
η_{ORC}		20.04	27.77	29.43	15.81	18.96	20.61
Process unit	Mechanical ($\dot{W}$) or thermal ($\dot{Q}$) power (MW) [a]						
RC_TURBINE	$\dot{W}$(outgoing)	38.98	38.98[b]	–	40.69	40.69[b]	–
RC_COOLER then RC_CONDENS	$\dot{Q}$(outgoing)	25.11	25.11	25.11	25.11	25.11	25.11
RC_COND_COOL	$\dot{Q}$(outgoing)	126.22	73.54	65.84	176.80	136.94	120.93
RC_PUMP	$\dot{W}$(ingoing)	1.06	1.06	0.98	2.77	2.77	2.50
RC_BOILER	$\dot{Q}$(ingoing)	189.25	136.57	91.91	239.83	199.97	130.88
RC_REGEN	$\dot{Q}$(in- outgoing)	–	0.00	0.00	–	0.00	0.00
RC_TURBINE_1	$\dot{W}$(outgoing)	–	–	17.13[c]	–	–	16.77[c]
RC_RE_HEATER	$\dot{Q}$(ingoing)	–	–	36.96	–	–	53.08
RC_TURBINE_2	$\dot{W}$(outgoing)	–	–	21.78[c]	–	–	23.65[c]
RO_PUMP	$\dot{W}$(ingoing)	4.80	4.80	4.80	4.80	4.80	4.80
TURB_REC_RO	$\dot{W}$(outgoing)	1.88	1.88	1.88	1.88	1.88	1.88

[a] Ingoing and outgoing from the working fluid side. [b] Mechanical work ($\dot{W}/\dot{m}$ in kJ/kg) generated by RC_TURBINE in configuration 2 of the ORC: 136 for EB and 86 for IP.

[c] Mechanical work ($\dot{W}/\dot{m}$ in kJ/kg) generated by RC_TURBINE_1 and RC_TURBINE_2 in configuration 3 of the ORC: 147 for EB and 95 for IP.

pressure, the only external thermal energy addition required to cause evaporation in the first effect is supplied conventionally by fossil fuel combustion and more occasionally by solar energy [18]. The vapors thus formed which are used to heat the feed (sprayed seawater) of the next effect are practically free of salts and lead after flowing through the LTMED condenser to a pure water distillate. At the same time, the brine accumulating at the bottom of each effect and circulating from the first to the last one is a non-desirable byproduct with a negative impact for environment, similarly to the brine from the RO process [9,17,19]. Nevertheless, thanks to decreasing levels of pressure (and thus temperature) applied to each effect, the latent heats of the produced vapors in the previous effects are successively reused for the next effects [18,19]. Another advantage of operating under low temperature is a reduction of fouling outside of the tubes inducing minimal maintenance and little pre-treatment of seawater [7]. Moreover, it is worth mentioning that commonly the first three effects of a LTMED process are the most effective [40] and that the contribution of the final cost of drinking water is higher for the distillate produced in the last effect [41].

Hence, combining the RO and LTMED technologies in the same site should mitigate their drawbacks and offer to use common intake and outfall facilities with a consequent decrease in the cost of civil works, in pumping energy and in exergy destruction. While the simplest level of hybridization involves the blending of product coming from the two technologies, higher levels were proposed in the literature where either the outlet flow of the LTMED condenser enters the RO process (exploiting thus beneficial effect of temperature on RO membrane performance as observed experimentally in **Appendix A**) [1,38] or the RO permeate enters into the LTMED process (reducing the number of stages required in the RO process to achieve the desired water quality) [42].

Therefore, as shown in Fig. 1, the RO unit was modelled by a splitter dividing the RO pump output in two streams, on one hand the permeate brought back to the atmospheric pressure via a valve for producing the

Table 4
Exergy analysis after simulation of the solar polygeneration plant integrating the various ORC configurations tested.

Exergy destruction rate (MW)	Working fluid					
	EB			IP		
	ORC configuration			ORC configuration		
	1	2	3	1	2	3
$\dot{E}x_d$(*RC_TURBINE*)	2.80	2.80	–	3.60	3.60	–
$\dot{E}x_d$(*RC_COOLER*)then $\dot{E}x_d$(*RC_CONDENS*)[a]	7.95	3.84	3.84	4.43	2.51	2.51
$\dot{E}x_d$(*RC_COND_COOL*)	4.84	1.74	1.56	3.83	2.69	2.37
$\dot{E}x_d$(*RC_PUMP*)	0.13	0.13	0.12	0.61	0.61	0.55
$\dot{E}x_d$(*RC_BOILER*)	21.70	9.72	4.82	18.70	12.40	6.66
$\dot{E}x_d$(*RC_REGEN*)	–	1.68	3.07	–	0.99	2.90
$\dot{E}x_d$(*RC_TURBINE_1*)	–	–	1.20	–	–	1.30
$\dot{E}x_d$(*RC_RE_HEATER*)	–	–	2.47	–	–	4.41
$\dot{E}x_d$(*RC_TURBINE_2*)	–	–	1.40	–	–	1.90
$\dot{E}x_d$(*ORC*)	37.42	19.91	18.47	31.17	22.80	22.60
$\dot{E}x_d$(*Solar polygeneration plant*)	40.27	22.79	21.25	34.02	25.64	25.49

[a] Heat exchanger named RC_COOLER for the ORC configuration 1, then RC_CONDENS for the ORC configurations 2 and 3.

desired desalted water, and on the other hand the high-pressure brine routed to an energy recovery Pelton turbine [43]. The resulting brine under atmospheric pressure is then sent into a second splitter to produce on one hand the RO residual brine and on the other hand the RO brine recycled to the LTMED process of which was only modelled the first effect (SEP_EFF_1) with its evaporator. This one is played by part of the ORC condenser (RC_COND_COOL) where the working fluid cooling and condensing (hot-side stream) partially vaporizes the RO recycled brine (cold-side stream). The further effects, similarly fed in parallel with residual RO brine, were drawn in dash line only to depict one of the possible options taking advantage of the two desalination technologies (as analyzed in the previous paragraph). This option enables to increase the drinking water production and to improve the overall product quality by blending the permeate and distillate, while reducing not only the investment costs with a single RO stage but also mineral addition to the distillate to make it drinkable. Note that in this option a supplemental seawater stream used as cold source in the condenser of the LTMED process may be added to the RO feed as proposed in the literature to improve membrane performance by increasing operational temperature [1,38]. Also, the distillate from the LTMED process may be used to mitigate the fouling phenomenon appearing with time in the RO process.

2.4. Modelling specifications, simulation procedure and performance evaluation

On the basis of the case studies achieved in Venezuela and northern Chile by **Mata-Torres et al.** [7] and in Spain by **Bruno et al.** [28], we considered in this work a city of 100,000 inhabitants in the Middle East and North Africa, having an average electricity consumption of 35 MWe and drinking water requirements of around 300 kg/s; the HTF mass flowrate through the PTCs (RC_BOILER) operating under 1 bar being 1440 kg/s. The solar polygeneration plant producing the desired needs in electricity and drinking water has been considered 24 h operation. The specifications related to the solar PTCs, the ORC, and the hybrid RO-LTMED desalination process that are required for modelling and simulating the whole plant are gathered in Table 2 by referring to the plant units modelling shown in Fig. 1. The inlet stream temperature of the PTCs was selected as low as possible while checking that no state change occurs for the HTF and that the pinch temperature difference in the heat exchanger RC_BOILER playing the PTCs is superior or equal to 5 °C (as adopted in the literature for evaporator and condenser in ORCs, [44]). Similarly, the outlet pressure of the ORC turbine (RC_TURBINE) and of the valve recycling the brine from the RO process to the LTMED (B_VALVE) were selected so that the pinch temperature difference in the heat exchanger RC_COND_COOL playing part of the ORC cold source and the hot source of the LTMED is at least 5 °C [44].

For simulation of the whole solar polygeneration plant, two parameters were determined by using the Feedback Controller of PROII [30]. The first is the RO brine splitter specification on the recycled brine stream (eq. (1)) which was determined to obtain a vaporized mole fraction in the feed of the LTMED (PROD_EFF_1 stream) sufficient to ensure the proper operating of several effects. A high-value and low-value have been selected for this vaporized mole fraction (0.8 and 0.3 [45]) depending on the targeted level of concentration for the ultimately rejected brine.

$$Spec(\text{B\_SPLITTER}) = \dot{m}_{BRINE\_RECYC}/\dot{m}_{BRINE\_ATM} \tag{1}$$

expressing the ratio of RO brine stream that is recycled to the LTMED in terms mass flowrates ($\dot{m}_{BRINE\_RECYC}$ for the RO brine recycled to the LTMED and $\dot{m}_{BRINE\_ATM}$ for the brine leaving the RO process at atmospheric pressure and entering the RO brine splitter, Fig. 1).

The second parameter to be determined is the mass flowrate of the ORC working fluid determined so that the net power output for the whole solar polygeneration plant be equal (after conversion through an alternator) to the targeted electricity need 35 MWe. This net power output results from the mechanical powers delivered by both the ORC turbine (major contribution) and the RO energy recovery Pelton turbine to which it is necessary to subtract the powers required to drive the ORC pump and the RO pump, since the solar plant should be self-sufficient in energy:

$$\dot{W}_{RC\_TURBINE} + \dot{W}_{TURB\_REC\_RO} - \dot{W}_{RC\_PUMP} - \dot{W}_{RO\_PUMP} = 35\ (\text{MWe}) \tag{2}$$

where all variables are positive.

The most dominant factors influencing the performance improvement of a solar ORC are net power output, vapor expansion ratio across the turbine, thermal efficiency, and exergy efficiency of the cycle (where exergy is destroyed due to irreversibility taking place in the process) [11,46,47]. The first two factors were set as just mentioned above. Therefore, thermal efficiency (eq. (3)) and exergy destruction rate (eq. (4)) were selected to evaluate the performance improvement of the various solar ORC-RO-LTMED schemes investigated. The thermal efficiency of the ORC can be expressed as:

$$\eta_{ORC} = \frac{\dot{W}_{net}}{\dot{Q}_{RC\_BOILER}} = \frac{\dot{W}_{RC\_TURBINE} - \dot{W}_{RC\_PUMP}}{\dot{Q}_{RC\_BOILER}} \tag{3}$$

where $\dot{W}_{net}$ is the net mechanical power produced by the ORC and $\dot{Q}_{RC\_BOILER}$ is the total thermal power supplied to the ORC (by the solar PTCs). Regarding the exergy destruction rate $\dot{E}x_d$, this can be formulated, according to the second law of thermodynamics related to a steady-state process, as:

$$\sum_{i=in}\dot{W}_i + \sum_{i=in}\dot{Q}_i\left(1-\frac{T_{ref}}{T_i}\right) + \sum_{i=in}\dot{m}_i\overline{E}x_i = \sum_{j=out}\dot{W}_j + \sum_{j=out}\dot{Q}_j\left(1-\frac{T_{ref}}{T_j}\right) + \sum_{j=out}\dot{m}_j\overline{E}x_j + \dot{E}x_d \tag{4}$$

Table 5
Impact of the vaporized mole fraction in the feed of the LTMED (1rst effect). Results are given for a vaporized mole fraction of 0.3 (0.8 in parenthesis [a]).

Parameter	Working fluid					
	EB			IP		
	ORC configuration			ORC configuration		
	1	2	3	1	2	3
$\dot{m}_{BRINE\_RECYC}/\dot{m}_{BRINE\_ATM}$	0.48 (0.21)	0.28 (0.12)	0.25 (0.11)	0.73 (0.29)	0.57 (0.23)	0.50 (0.20)
$\dot{m}_{BRINE\_RESID}$(kg/s)	155 (238)	215 (264)	224 (268)	80 (211)	129 (231)	149 (239)
$\dot{m}_{PROD\_EFF\_1}$(kg/s)	145 (62)	85(36)	76(32)	220 (89)	171 (69)	151 (61)
$\dot{m}_{D\_EFF\_1}$(kg/s)	43 (50)	25 (29)	23 (26)	66 (71)	52 (55)	45 (49)
$\dot{m}_{B\_EFF\_1}$(kg/s)	102 (12)	60 (7)	53 (6)	154 (18)	119 (14)	106 (12)
$\dot{E}x_d(ORC)$(MW)	38.2 (37.4)	20.4 (19.9)	18.8 (18.5)	31.5 (31.2)	23.1 (22.8)	22.8 (22.6)
$\dot{E}x_d(solar\,plant)$(MW)	41.0 (40.3)	23.2 (22.8)	21.6 (21.3)	34.4 (34.0)	25.9 (25.6)	25.7 (25.5)

[a] Vaporized mole fraction value adopted in the feed of the LTMED (1rst effect) displayed on Figs. 3, 5 and 6.

where $\dot{W}_{i\,(j)}$ and $\dot{Q}_{i(j)}$ are the ingoing (outgoing) mechanical and thermal power exchange (all counted positively), $\overline{Ex}_{i(j)} = \overline{H}_{i(j)} - T_{ref} \cdot \overline{S}_{i(j)}$ and T_{ref} is the reference temperature used for calculating the mass exergy $\overline{Ex}_{i(j)}$ from the mass enthalpy $\overline{H}_{i(j)}$ and the mass entropy $\overline{S}_{i(j)}$ of the ingoing (outgoing) streams crossing the process boundary. In this work, $T_{ref} =$ 293.15 K and eq. (4) applied to the ORC and to the whole solar polygeneration plant (Fig. 1 with the LTMED limited to the first effect) led to expressions (5) and (6) respectively.

$$\dot{E}x_d(\mathrm{ORC}) = (\overline{E}x_{SOLAR\_1} + \overline{E}x_{SEA\_WATER} + \overline{E}x_{FEED\_EFF\_1}) - (\overline{E}x_{SOLAR\_2} + \overline{E}x_{SW2} + \overline{E}x_{PROD\_EFF\_1}) + \dot{W}_{RC\_PUMP} - \dot{W}_{RC\_TURBINE} \tag{5}$$

$$\dot{E}x_d(\text{whole plant}) = (\overline{E}x_{SOLAR\_1} + \overline{E}x_{SEA\_WATER}) + (\dot{W}_{RC\_PUMP} + \dot{W}_{RO\_PUMP}) - (\overline{E}x_{SOLAR\_2} + \overline{E}x_{DESAL\_WATER} + \overline{E}x_{BRINE\_RESID} + \overline{E}x_{D\_EFF\_1} + \overline{E}x_{B\_EFF\_1}) - (\dot{W}_{RC\_TURBINE} + \dot{W}_{TURB\_REC\_RO}) \tag{6}$$

where the ingoing (outgoing) streams are referred according to Fig. 1. The exergy balance equations for each unit are available in **Appendix B** (together with the corresponding mass and energy balance equations).

3. Results and discussion

Simulation results obtained with ProII [30] for the solar polygeneration plant integrating the base ORC (configuration 1) or the two supplemental configuration proposals are given concisely on Figs. 3 and 5-6 respectively and in detail in **Appendix C**. Moreover, these results are given for both working fluids tested of which the corresponding *T-s* diagrams are depicted on Fig. 4. The thermal analysis and exergy analysis are displayed respectively in Tables 3 and 4, for all configurations with each working fluid; the analysis of the ORC heat exchangers aiming to check the absence of any temperature profile cross-over and a pinch temperature difference superior or equal to 5 °C [44] between the hot-side and the cold-side streams of the exchangers is detailed in **Appendix D**. The impact of the vaporized mole fraction in the feed of the LTMED first effect is shown on Table 5.

3.1. Evaluation of the base ORC (configuration 1)

As observed on Fig. 3, the inlet stream conditions selected for the PTCs (Section 2.4) lead to operate with a vapor state HTF when EB is the ORC working fluid, but with a liquid state HTF when IP is the ORC working fluid. However, it should be noted that changing the temperature of the PTC inlet stream has no impact on the thermal efficiency of the ORC (due to the simulation procedure adopted to determine the mass flowrate of the working fluid, eq. (2)), but it does influence the exergy destruction rate of the ORC and then of the solar polygeneration plant (because of the temperature difference induced between the hot-side and cold-side streams of the RC_BOILER unit playing the PTCs). Moreover, whatever the ORC working fluid, EB or IP, the turbine inlet temperature is far below the limit temperature recommended to insure any organic fluid be chemically stable (325 °C, [35]). Also, the saturation temperature in the first effect of the LTMED is similar to the value obtained by **Mata-Torres et al.** [7] as well as other related studies (65 °C, [41,45]). Of course, this saturation temperature is independent of the vaporized mole fraction (VP) selected for the LTMED feed (0.8 or 0.3) of which changes impact only the mass flowrates of the RO brine related streams and to a far lesser extent, the exergy destroyed inside the ORC and the solar plant (Table 5). On the basis of the chosen specification for the recycled RO brine stream (eq. (1)), decreasing VP leads to produce less residual RO brine by recycling it in a larger amount to feed the LTMED (stream BRINE_RECYC, FEED_EFF_1, then PROD_EFF_1), which results in a major increase of the concentrated brine production and a slight reduction of the distillate flowrate (streams B_EFF_1 and D_EFF_1, respectively). Indeed, the part of the water heat of vaporization removed from the thermal power absorbed by the recycled brine (RC_COND_COOL) needs to be compensated by an increase of the brine flowrate (the temperature and pressure conditions of the RO brine streams being independent of VP remain unchanged). As low levels of salts in the concentrated brine may be expected for low values of VP (0.3), existing devices could be used in this option. By contrast, new devices made in specific material (hyper-duplex stainless-steel, [17]) should be used for high values of VP (0.8) because of corrosion risks induced by higher levels of salts in the concentrated brine. Moreover, the operating points displayed on the *T-s* diagrams for the two working fluids, EB and IP (Fig. 4a), illustrate the appropriate thermodynamic behavior of the ORC. Indeed, after expansion of the saturated vapor (point 1) through the turbine (RC_TURBINE), the outgoing superheated vapor fluid (point 2) is first partly cooled down by the RC_COOLER unit (point 4) to be entirely cooled and condensed, then subcooled by the RC_COND_COOL unit (point 5), these two heat exchangers modelling the ORC cold source; the subcooled liquid working fluid is then pumped up to the RC_BOILER inlet (point 6) for complete vaporization before entering the turbine (RC_TURBINE).

The thermal efficiencies of the ORC obtained by using EB or IP as working fluid are respectively 20 and 16%; the same net power is provided by both fluids, but much lower thermal power (of about 21%) is required from the PTCs with EB (Table 3). In addition, the required mass flowrate of the working fluid through the ORC is 39% lower for EB than for IP. Exergy destruction rate inside the ORC is lower when using EB rather than IP as working fluid (37 and 31 MW, respectively), with 3 MW increase of the exergy destruction rate inside the solar plant due to the irreversibility of the RO process (Table 4; RO_PUMP, Fig. 3). As expected, the larger part of exergy destroyed (about 58%) occurs in the PTCs (RC_BOILER) and to a much smaller extent in the first and second units modelling the ORC cold source (RC_COOLER and RC_COND_COOL) because of the temperature differences between the hot-side and cold-side streams of the corresponding heat exchangers.

However, in the base ORC (Fig. 3) the working fluid is cooled down by the seawater to be heated again by the HTF. Therefore, a second configuration was proposed for the ORC where the hot working fluid outgoing the turbine (RC_TURBINE) would pre-heat the cold working fluid ingoing the PTCs (RC_BOILER) in order to reduce their thermal contribution in the ORC.

3.2. ORC with a regenerator (configuration 2)

In this second ORC configuration (Fig. 5), the heat exchanger RC_REGEN insures the thermal transfer between the two hot-side and cold-side streams containing the same fluid, EB or IP, but in two different states: a superheated vapor outgoing the ORC turbine (RC_TURBINE) under low-pressure and delivering its thermal energy to a subcooled liquid under high-pressure before entering the PTCs (RC_BOILER). Based on the self-heat recuperation technology [48], this specific heat exchanger works like a thermal regenerator. The RC_REGEN operating conditions were specified so that (Table 2): (*i*) no

Table 6
Summary of the cost analysis focused on the ORC system by giving the installed costs of the different equipment. Results are given for a vaporized mole fraction of 0.8 (0.3 in parenthesis) in the feed of the LTMED (1rst effect).

Parameter	Working fluid					
	EB			IP		
	ORC configuration			ORC configuration		
	1	2	3	1	2	3
•Installed cost for each equipment (k€ 2019)						
RC_TURBINE	29,749	29,749	–	30,833	30,833	–
RC_COOLER then RC_CONDENS	517	96	96	1187	132	132
RC_COND_COOL [a]	701 (319)	1035 (471)	932 (424)	2400 (1091)	3383 (1538)	2916 (1325)
RC_PUMP	1496	1496	1387	3371	3371	3053
RC_BOILER	4883	3286	2815	882	830	613
RC_REGEN	–	7949	9936	–	8942	12,917
RC_TURBINE_1	–	–	14,987	–	–	14,724
RC_RE_HEATER	–	–	1094	–	–	2059
RC_TURBINE_2	–	–	18,310	–	–	19,612
•Total installed cost (M€ 2019)	37.435 (36.963)	46.611 (43.046)	49.558 (49.049)	38.673 (37.364)	47.492 (46.647)	56.026 (54.435)
•CAPEX (M€ 2019)	67.2 (66.5)	78.5 (77.5)	89.2 (88.3)	69.6 (67.3)	85.5 (82.1)	100.8 (98.0)
•Electricity (M€ 2019/year)	15.168	15.168	15.168	15.168	15.168	15.168
•Payback time (year)	4.43 (4.39)	5.18 (5.11)	5.88 (5.82)	4.59 (4.43)	5.64 (5.42)	6.65 (6.46)

[a] RC_COND_COOL is made of carbon steel when the vaporized mole fraction is 0.3 but of 316 stainless steel, a corrosion resistant and thus more expensive material, when the vaporized mole fraction is 0.8.

pressure change occurs along the heat exchanger; (*ii*) the hot-side outgoing working fluid RC3 be at its dew point. Thanks to theses specifications, the thermal profiles of the regenerator show no cross-over between the hot-side and cold-side streams with a temperature difference always superior or equal to 5 °C [44]). Another consequence of the specifications adopted for RC3 stream is that the heat exchanger playing the first part of the ORC cold source becomes in this second configuration a full condenser (RC_CONDENS, Fig. 5). Thus, operating conditions of all streams are unchanged compared to configuration 1 of the ORC, excepting the stream RC4 outgoing the RC_CONDENS unit and the two additional streams RC3 and RC7 introduced by the implementation of the regenerator. As a result, the operating conditions of the PTC outlet stream SOLAR_2 changed also, the brine and distillate flowrate production included (Fig. 5).

The *T-s* diagrams of the two working fluids evaluated, EB and IP, show clearly the impact of the regenerator which, by assuming part of the PTC thermal contribution, brings up the working fluid from point 6 to point 7 (representing respectively the streams RC6 and RC7) (Fig. 4b). The thermal power required from the PTCs being lower, the ORC thermal efficiency is higher for this second configuration than for the precedent, whatever the working fluid analyzed: 28% for EB and 19% for IP (Table 3). Simultaneously, similar improvement is observed regarding the exergy destruction rate in this second configuration of the ORC with a decrease of 47% for EB and 27% for IP compared to configuration 1 (Table 4); the most significant enhancement being obviously observed for the PTCs. The regenerator impacting RC4 stream operating conditions, productions of the brine and distillate are also affected. Whereas the residual brine flowrate increases compared to configuration 1 of the ORC, less brine is recycled to the LTMED process which delivers then less distillate and concentrated brine; and this whatever the working fluid considered (Table 5).

Nonetheless, isothermal expander/turbine is usually more effective than adiabatic expander/turbine by generating a higher power; for this reason, a third ORC configuration was proposed as described in the following section.

3.3. *ORC with a regenerator and a double-stage turbine (configuration 3)*

With the aim of approaching the isothermal expander, the ORC turbine (RC_TURBINE) was changed for a double-stage turbine of the same isotropic efficiency ($\eta = 0.90$) with an intermediary reheater to bring back the inlet temperature of the second-stage (RC2_1) to the inlet temperature of the first-stage (RC1) (Fig. 6). The PTCs were used to play the hot source of the reheater; thus, an additional feed of HTF, specified with reference to the inlet stream of the RC_BOILER unit, was directed to flow inside the hot-side of the reheater (Fig. 6). Moreover, when sizing a

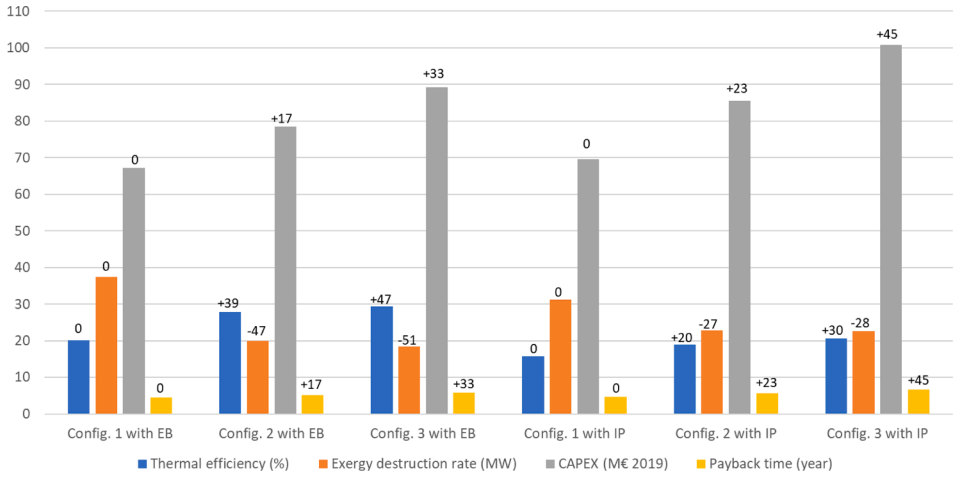

Fig. 7. Economic analysis vs thermodynamic analysis of the various ORC designs investigated with the working fluids EB or IP (figures given on the bars are percent improvements with respect to the base ORC (configuration 1)).

double-stage turbine, the optimal single-stage pressure ratio leading to maximize the mechanical power generated is defined as the square root of the overall pressure ratio [12]. Consequently, the outlet pressure specified for the first-stage turbine in this third configuration of the ORC was set to 2.24 bar for EB working fluid; 8.12 bar for IP (Fig. 6; Table 2). Thus, compared to configuration 2 of the ORC, the streams affected by changes made here are: the outlet streams of the turbine second-stage and regenerator RC3 and RC7, not to mention the new additional streams RC2_1 and RC2_2.

As observed on the *T-s* diagrams of the working fluids EB and IP where point 7 (representing RC7 stream) is moved upper in temperature, the impact of the double-stage turbine with intermediary reheater is significant on the regenerator limiting even more the thermal contribution from the PTCs to the ORC (Fig. 4c). As expected, the mechanical work generated by the double-stage turbine is higher than the mechanical work generated by the single-stage turbine of the previous ORC configuration (improvement of 8% and 10% for EB and IP respectively; Table 3). As a result, the thermal efficiency of the ORC within this third configuration is even more improved, reaching 29% and 21% for EB and IP respectively. In addition, this improvement goes with a slight reduction of the working fluid flowrate (8% for EB, 10% for IP; Table 3). The exergy destruction rate also decreases compared to configuration 2 of the ORC, more for EB working fluid than for IP (decrease of 7% and 1%, respectively) (Table 4). The second part of the ORC cold source requiring less thermal power than for the previous configurations, a larger production of residual brine is obtained while the amount of recycled brine to the LTMED decreases, inducing a reduced production of concentrated brine and distillate (Table 5).

3.4. Economic analysis of the ORC configurations investigated

This economic analysis aims at giving a preliminary estimation of the capital cost and of the payback time for each ORC design investigated with the two working fluids (EB or IP) in order to determine the optimal combination resulting from a compromise between benefits based on thermodynamic criteria (maximum energy efficiency and minimum exergy destruction) and drawbacks based on economic criteria which are however weighable considering the payback time.

The techno-economic evaluation of the different case studies (the three ORC configurations with EB or IP as working fluid) is performed with the factorial Pre-Estime method [49] developed to roughly evaluate the cost of basic engineering projects. Factorial estimates are based on the idea that all categories of capital expenditures in a plant are related to the cost of the purchased equipment. The equipment cost is thus evaluated through a correlation function of its main sizing parameters and is multiplied by correction factors considering for instance the installation costs, the material type, the level of pressure in the equipment (among other parameters). Due to the use of averaged correlations, the uncertainty of the method is relatively high. Equipment purchased costs have been used from the literature data, exclusively from **Chauvel et al.** [49] to guarantee the homogeneity of the evaluation. The installation factor considers foundations, structures, buildings, electrical installation, instrumentation, insulation, painting, etc. This factor is a function of the considered equipment. The environment factor considers storage units, administrative services, engineering costs, contingency charges, financial costs, etc.

The following assumptions are considered for calculations:

- The boundaries of the analysis are limited to the ORC system only.
- The used cost functions are expressed in € from year 2000.
- The Chemical Engineering Plant Cost Index (CEPCI) is used to consider the evolution of the costs as a function of time to estimate the purchase cost of each unit (Index $CEPCI_{2000} = 394.1$ and Index $CEPCI_{2019} = 607.5$). Finally, the currency used is expressed in € from 2019.
- Production time of 8000 h per year (capacity factor of 91.3%) is considered.
- The different installation factors are function of the type of equipment selected.
- The environment factor (f_e) considered for the entire plant is equal to 1.8 in this study because the plant is assumed to be located on an existing site which reduces its value.

The capital expenditures (CAPEX) are calculated according to equation (7):

$$\text{CAPEX} = f_e \left(\sum_k f_{g,k} \cdot f_{m,k} \cdot f_{p,k} \cdot C_k \right) \tag{7}$$

where f_e is the environment factor, $f_{g,k}$ and $f_{m,k}$ the installation and material factors of equipment k, $f_{p,k}$ the factor depending on the level of pressure in equipment k and C_k the purchased cost of equipment k (expressed in € from 2019). The payback time corresponds to the ratio of the CAPEX divided by the revenues of electricity for sale.

The summary of the economic analysis for the ORC system by giving the installed cost of each equipment is shown in Table 6 for the different case studies (configurations 1 to 3 with EB or IP as working fluid). The detailed results can be found however in **Appendix E** [49]. The RC_TURBINE represents the main contribution to the overall installed cost (between 63% and 83% depending on the case study). The turbine cost function depends on the outgoing mechanical power which is relatively high. The RC_PUMP corresponds to a lower share of the overall installed cost (between 3% and 9% depending on the case study). The considered pump is a centrifugal one and its cost function depends on the ingoing mechanical power. The rest of the installed cost is due to the contribution of the different heat exchangers (RC_COOLER, RC_CONDENS, RC_BOILER, RC_REGEN, RC_RE_HEATER) which are considered as counter-current shell and tubes heat exchangers (with a basic TEMA configuration: AES). The cost of a heat exchanger depends on its exchange surface which is determined knowing the 4 inlet/outlet temperatures (to calculate the average logarithmic temperature difference) and assuming a reasonable order of magnitude of the overall heat transfer coefficient for each exchanger. The presence of the RC_REGEN gas/liquid heat exchanger (that enables the thermal integration) implies also a significant additional cost for configurations 2 and 3. This equipment cost is high due to a relatively low overall heat transfer coefficient (important limitation to heat transfer on the gas side) and a high exchanged thermal power (between 40 and 82 MW) implying finally a high exchanger area and then a high installed cost. Similarly, it should also be mentioned that the RC_BOILER cost is higher using EB than IP as working fluid due to the HTF which is in gas state for EB (liquid for IP). Nevertheless, the thermal power of the RC_BOILER being lower when working with EB (Table 3), one can reasonably assume that this additional cost of the RC_BOILER should be compensated by a reduced cost of the solar field. In addition, the overall installed cost of configuration 3 itself is higher than the one of configuration 2 due to the presence of the RC_RE_HEATER. The material considered for each equipment (turbine, pump, heat exchangers) is carbon steel except for the RC_COND_COOL with a vaporized mole fraction of 0.8 whose material is 316 stainless steel to be corrosion resistant [50,51]. Overall, for a given working fluid, the CAPEX increases from configuration 1 to 3 mainly due to the presence of supplementary heat exchangers used for the thermal integration. For a given ORC configuration, the CAPEX is always higher for IP compared to EB. This is mainly due to a higher flowrate of working fluid flowing in the ORC, implying that some equipment is larger and involves then a higher cost. These results are confirmed by the payback time that considers the revenues due to the sale of the produced electricity.

Thus, as illustrated by Fig. 7, both the thermodynamic and economic criteria designate EB as a better working fluid than IP. However, the decision regarding the optimal ORC design may be subject to discussion

when considering that the major improvements in terms of thermal efficiency and exergy destruction rate are brought by the implementation in the base ORC of the regenerator (configuration 2) and to a lesser extent by the replacement of the single-stage turbine by a double-stage turbine combined with an intermediary reheater (configuration 3); with, for each configuration change, the same CAPEX increase. Considering the reasonable payback times (less than 6 years, Table 6) and the environmental benefits induced by further thermal integration, the last proposal for the ORC design (configuration 3) should be however the most appropriate.

4. Conclusion

Performance evaluation of various ORC designs on the basis of thermodynamic criteria (maximum energy efficiency and minimum exergy destruction) followed by an economic analysis led to identify the best configuration implementing into the base ORC both a regenerator and a double-stage turbine combined with an intermediary reheater. The regenerator contributing mainly to the ORC improvement, the alternative without the double-stage turbine and intermediary reheater has also been detailed and thus could be used in case of limited cost-investments. Among the two working fluids evaluated during the ORC simulation, ethyl butanoate proposed as green alternative to isopentane commonly used for such applications revealed to be the most performant, improving the thermal efficiency by 43% and the exergy destruction rate by 18% for the ORC incorporating the double-stage turbine with intermediary reheater, in addition of the regenerator. This result could be reached thanks also to the hybrid RO-LTMED desalinization scheme adopted where the brine from the RO unit was routed to the LTMED, in line with the zero-liquid-discharge concept. Two alternatives considering the production of low- or highly- salt content brine depending the ultimate fate dedicated for the product (aquaculture or solar ponds/sodium batteries/HCl + NaOH production) were also proposed.

Thus, results obtained in this work illustrate that solar polygeneration systems with PTCs can be sustainable and viable systems for application in the future energy commodities and, when combined with RO-LTMED, for providing fresh water to population suffering water stress while creating wealth locally.

CRediT authorship contribution statement

Hadrien Jaubert: Conceptualization, Methodology, Software, Investigation, Writing - original draft. **Philippe Borel:** Validation, Resources, Supervision. **Pierrette Guichardon:** Methodology, Investigation, Writing - review & editing. **Jean-François Portha:** Formal analysis, Writing - review & editing. **Jean-Noël Jaubert:** Review, Resources, Funding acquisition. **Lucie Coniglio:** Conceptualization, Software, Writing - review & editing.

Declaration of Competing Interest

The authors declare that they have no known competing financial interests or personal relationships that could have appeared to influence the work reported in this paper.

Acknowledgments

The authors would like to express their acknowledgments to MSc Mireille Argeme from Centrale Marseille (France) for her technical support during reverse osmosis experiments, Dr. Benjamin Gury from SLCE Watermakers (France) and Professor Ahmed Farouk Abdel Gawad from Zagazig University (Egypt) for their helpful discussions during the work, and Dr. Rolando Bosleman from Energy Recovery (United States) for his information regarding energy recovery pressure exchanger operating conditions.

Appendix A. Reverse osmosis (RO) experiments

The experiments planned to obtain the required information for modelling and simulating the RO unit of the solar polygeneration plant investigated to produce electricity and drinking water by a hybrid desalination system, were carried out with a bench scale RO unit specific to spiral-wound membranes. The whole of the set up was already used in previous studies (Fig. A1) [13]. A polyamide thin-film composite RO spiral-wound module type BW30-2540 was selected since typically adopted in industry for its operating reliability and the water quality it usually produces [14]. The technical characteristics of the module were: 1.016 m long, 0.099 m diameter, spacer-filled channels with a full height of 8.636×10^{-4} m, and a filtration area of 7.6 m^2. The membrane module was installed vertically with all streams flowing downwards [13].

In this pilot, the saline water stored in a feed tank of 0.1 m^3 capacity *(1)* is routed under pressure via a centrifugal pump *(13)* up to the inlet of the RO module *(4)* for leading to the permeate (purified water) and retentate (brine) at the outlet. There, permeate *(2)* and retentate *(3)* flow each through rotameters *(5–6)* before being recycled into the storage tank (or feed tank). The temperature of the storage tank is controlled manually with a cooling coil fed with municipal water. In addition of permeate and retentate volume flowrates (Q_P and Q_R, respectively) measured from rotameters *(5–6)*, pressure gauges were also placed at the RO module inlet *(8)* and at the retentate outlet *(12)* in order to know there the experimental pressure (P_F and P_R, respectively). Different operating conditions of pressure and saline water feed flowrate can be imposed by playing on the needle valve controlling the retentate flow *(11)* and on the by-pass diaphragm valve *(9)* returning to the storage tank part of the feed saline water pumped (the remainder feeding the RO module *(7)* after flowing through a ball-type feed valve *(10)*). Such a closed cycle operating mode helps to maintain a constant salt concentration with time inside the feed storage tank.

Various operating conditions in terms of pressure and feed flowrate ($Q_P + Q_R$) were selected by applying increasing salt concentrations in the storage tank (C_F) maintained at constant temperature (T_F). For a given salinity, the saline solutions used as surrogates for seawater were prepared by adding a well-known amount of reagent-grade NaCl (Sigma-Aldrich, France) in distilled water produced from a homemade pilot. For each operating condition and once steady state is achieved (approximatively 1.5 h after pilot start up), samples from the storage tank *(1)* and the permeate *(2)* were withdrawn in order to follow by conductimetry their concentration in NaCl versus time. The conductivity meter used (Eutech/oakton CON 11, Singapore/USA) was equipped with an electrode with built-in temperature sensor (EC-CONSEN91W 35608–50) [14]. Samples were placed several minutes in a thermostatically-controlled water bath at 25 °C to be sure that all conductivity measurements be carried out at the same temperature. Calibration lines established at 25 °C were used to convert conductivities to concentrations.

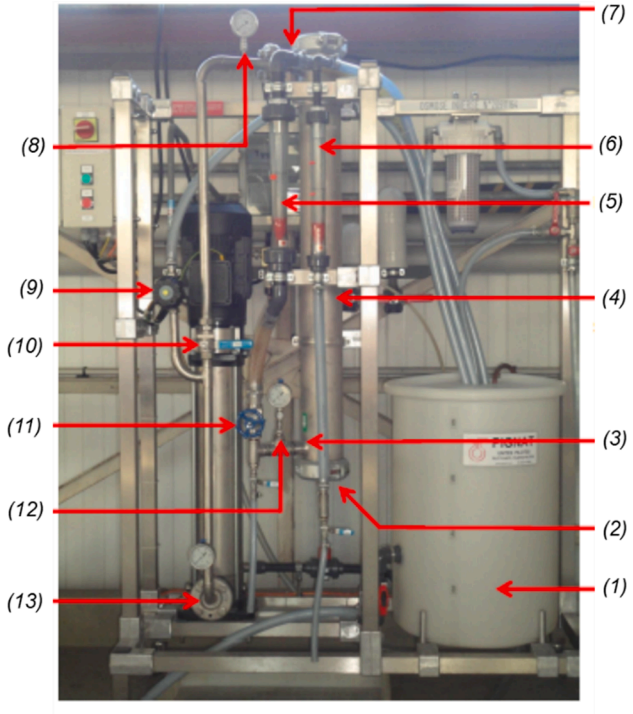

Fig. A1. Bench scale RO unit used for carried out the experiments presented in this work (PIGNAT OSM/2000, France). *(1)* saline water storage tank; *(2)* permeate outlet; *(3)* retentate outlet; *(4)* RO spiral-wound module type BW30-2540 (Dow Filmtec, USA); *(5)* retentate rotameter (KOBOLD KSA, Germany, 35 4030H K50); *(6)* permeate rotameter (KOBOLD KSA, Germany, 4006H K32); *(7)* saline water inlet; *(8)* inlet RO module pressure gauge; *(9)* by-pass diaphragm valve; *(10)* ball-type feed valve; *(11)* needle valve for controlling the retentate flow; *(12)* outlet retentate pressure gauge; *(13)* feed centrifugal pump (EBARA EVM3 26F5, Italy).

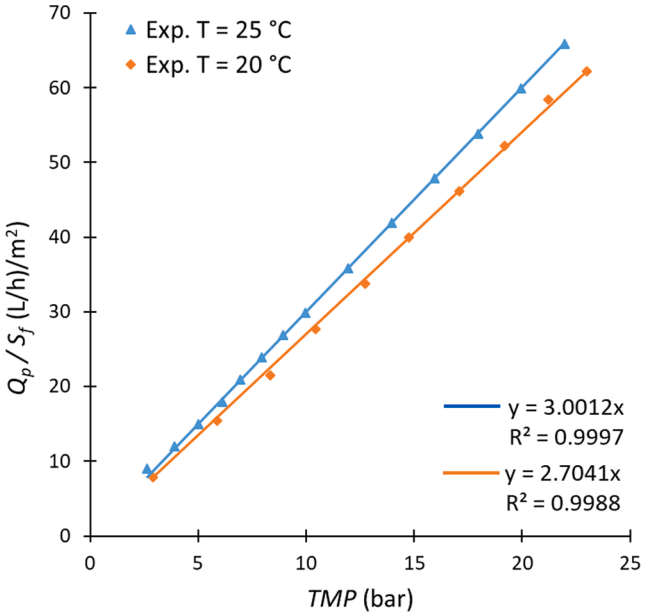

Fig. A2. Determination of the membrane permeability to pure water (solvent) and effect of temperature from the plot of the permeate volumetric flux versus the transmembrane pressure (RO spiral-wound module BW30-2540, Dow Filmtec, USA).

A1. Physico-chemical aspects of the RO unit and limiting factors

Solvent (pure water) and solute (NaCl) transmembrane transfers are described locally by the solution-diffusion model expressing the permeate volumetric flux (Q_P/S_f) by:

$$Q_P/S_f = A^{*}\cdot(TMP - \Delta\pi) \tag{A1}$$

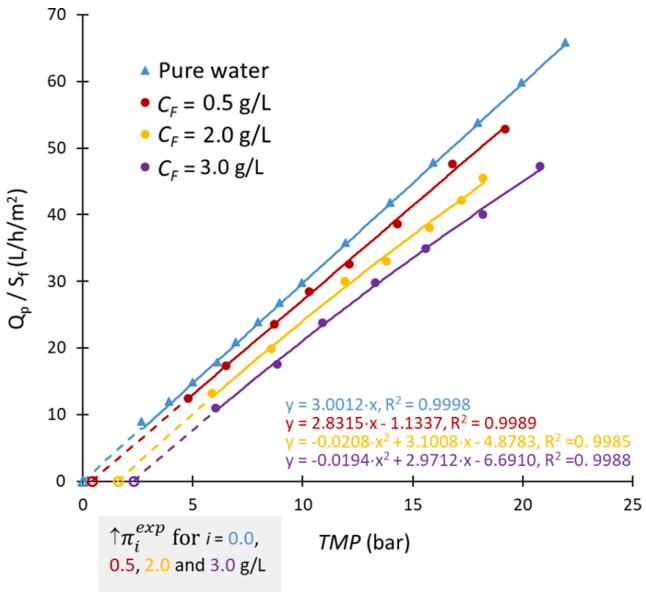

Fig. A3. Permeate volumetric flux versus transmembrane pressure for the treatment of various NaCl solutions at 25 °C (RO spiral-wound module BW30-2540, Dow Filmtec, USA). Patterns: experimental data; continuous lines: experimental data regression; dashed lines: linear approximation by van't Hoff's law; equations written in blue, red, yellow, and purple result from regression of the experimental data related to the treatment of saline solutions of NaCl concentration 0.0, 0.5, 2.0, and 3.0 g/L, respectively.

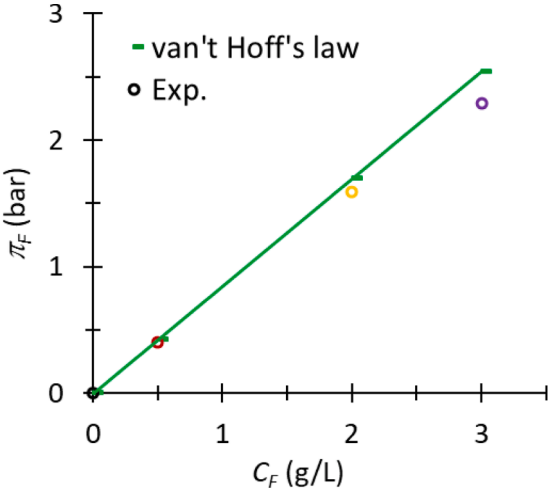

Fig. A4. Comparison between experimental osmotic pressure and van't Hoff's theory for various NaCl solutions maintained at 25 °C.

with

$$TMP = \frac{P_F + P_R}{2} - P_P \tag{A2}$$

In these expressions, Q_P is the permeate volume flowrate, S_f the membrane filtering surface, A^* the (intrinsic) membrane permeability to pure water, *TMP* the transmembrane pressure considered as the average pressures at the module inlet P_F and at the retentate outlet P_R, decreased by the permeate pressure P_P equal to 1 atm; $\Delta\pi$ is the osmotic pressure difference between the membrane-liquid interfaces. Since the permeate is very diluted, $\Delta\pi$ is assimilated to the feed saline water osmotic pressure π_F. For dilute solutions such as seawater, π_F can be estimated according to the Van't Hoff's law:

$$\pi_F = j\, R\, T_F\, C_F \tag{A3}$$

where $j = 2$ because NaCl is dissociated in distilled water in two different ions (Na^+ and Cl^-). R is the ideal gas constant and C_F is the molar concentration of NaCl in the saline water feed of which temperature is T_F.

A first set of experiments was carried out with the storage tank filled of distillated water (considered as the solvent "pure water") in order to plot the permeate volumetric flux measured for various *TMP* values and determine thus the membrane pure water permeability (A^*) from the slope of the straight line obtained. As observed in Fig. A2 gathering the experiments carried out at two temperatures with distilled water, a 5° increase of the feed water temperature leads to increase the membrane solvent permeability of 10%. This result may be explained by the expression relating variable A^* to the liquid water viscosity μ:

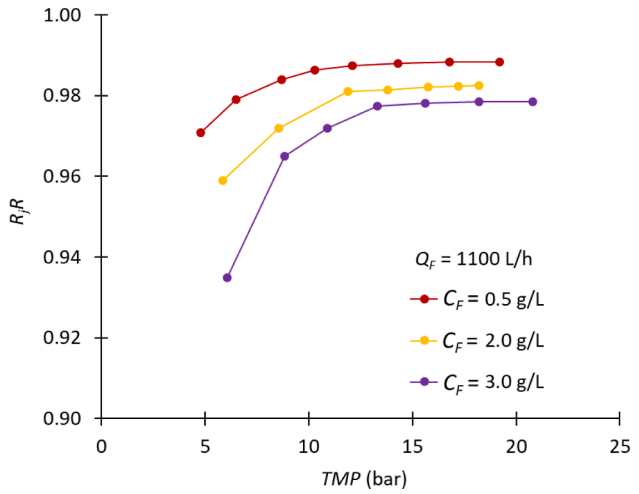

Fig. A5. Experimental NaCl rejection ratio versus transmembrane pression during the treatment of various NaCl solutions at 25 °C (RO spiral-wound module BW30-2540, Dow Filmtec, USA).

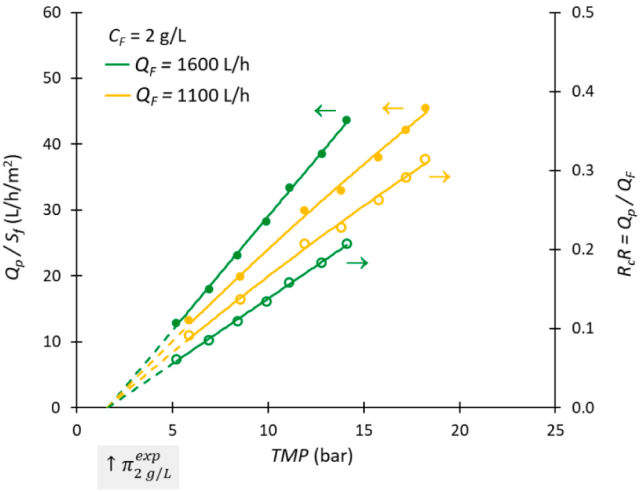

Fig. A6. Permeate volumetric flux and water recovery ratio versus transmembrane pressure for the treatment of a given NaCl solution at 25 °C – Effect of the feed salt water volume flowrate (RO spiral-wound module BW30-2540, Dow Filmtec, USA). Patterns: experimental data; continuous lines: experimental data regression; dashed lines: linear approximation by van't Hoff's law.

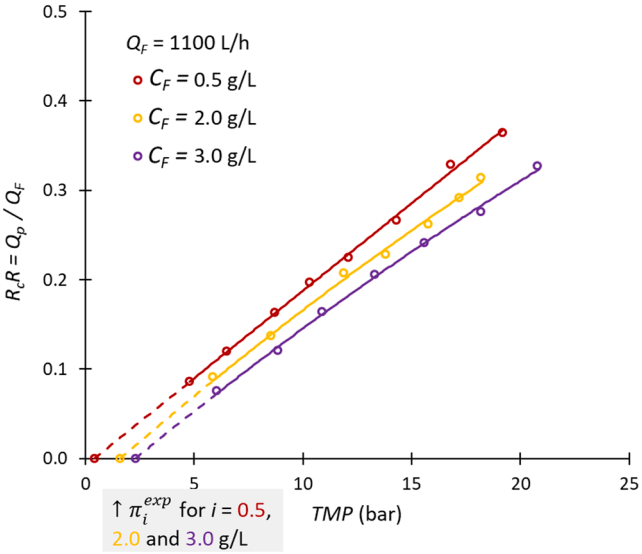

Fig. A7. Water recovery ratio versus transmembrane pressure during the treatment at a given feed saline water volume flowrate and at 25 °C – Effect of the NaCl concentration (RO spiral-wound module BW30-2540, Dow Filmtec, USA). Patterns: experimental data; continuous lines: experimental data regression; dashed lines: linear approximation by van't Hoff's law.

$$A^* = \frac{1}{\mu \cdot R_m} \tag{A4}$$

where μ is temperature dependent according to an Arrhenius type law and R_m is the intrinsic membrane resistance (temperature independent). Moreover, the membrane permeability to pure water obtained at 25 °C was: $A^* = 3.0\ \text{L}\cdot\text{h}^{-1}\cdot\text{m}^{-2}\cdot\text{bar}^{-1}$ (i.e. $A^* = 8.3 \times 10^{-12}\ \text{m}\cdot\text{s}^{-1}\cdot\text{Pa}^{-1}$). All this information agrees with studies carried out on similar membranes [1,37,38]. Since operating at 25 °C improves the process performance by increasing the membrane solvent permeability, this temperature was definitely adopted, i.e. for the following experiments and the modelling and simulation of the RO unit.

Fig. A3 shows the permeate volumetric flux versus the *TMP* applied for the treatment of various NaCl solutions at 25 °C. As it can be observed the membrane permeability decreases in presence of the solute NaCl retained. This result agrees with the resistances-in-series approach expressing variable A^* according to:

$$A^* = \frac{1}{\mu \cdot (R_m + R_s)} \tag{A5}$$

where the resistance of the retained salts R_s adds its contribution to the intrinsic membrane resistance R_m. Furthermore, at high *TMP*s, while the curves related to low salt concentrations remain linear, the other two curves tend to become slightly concave, particularly when the NaCl concentration increases. This decrease in permeate volumetric flux at high *TMP* is due to the fouling phenomenon which results from solute accumulation on the membrane surface. Indeed, the solute concentration being higher at the surface of the membrane than in the feed stream, it follows an increase in the osmotic pressure near the membrane and thus a decrease in the effective pressure $(TMP - \Delta\pi)$ involving a permeate volumetric flux decrease. Note that the effective pressure $(TMP - \Delta\pi)$ is the "vector" inducing the transfer of solvent through the membrane as concerns RO process.

Moreover, extrapolation of the obtained curves to a zero permeate volumetric flux provides the osmotic pressure of the feed at the corresponding NaCl concentrations. By plotting the experimental values thus obtained of the osmotic pressure with the theoretical values estimated from van't Hoff's law (Fig. A4), it can be observed that the theory tends to slightly overestimate the experiment when the salt concentration increases, but that the agreement is good at low concentrations. This observation is in line with the very diluted solution hypothesis of van't Hoff's law. As a result, for seawater containing 30 g/L of NaCl at 25 °C, it will be necessary to apply a *TMP* much higher than the osmotic pressure of 25 bar expected in theory, if willing to produce a satisfactory permeate flowrate.

Finally, after rinsing the pilot with distilled water, nearly the initial value of membrane pure water permeability was got back. It can therefore be concluded from this result that membrane fouling induced by concentration polarization can be mitigated, without stopping the unit, by a punctual circulation of pure water.

A2. Performance of the RO unit and optimal operating parameters

Performance of the RO unit may be evaluated by two key parameters i.e. the salt rejection ratio (R_jR, eq. A(6)) indicator of the RO unit selectivity and the pure water recovery ratio (R_cR, eq. A(7)) indicator of the liquid fraction crossing the membrane. Their expressions are:

$$R_jR = 1 - \frac{C_P}{C_F} \tag{A6}$$

$$R_cR = \frac{Q_P}{Q_F} \tag{A7}$$

where C_P (Q_P) and C_F (Q_F) are the NaCl concentration (volume flowrate) in the permeate and the saline water feed, respectively.

Fig. A5 and Figs. A6-A7 show respectively the R_jR and R_cR versus the *TMP* applied by varying either the NaCl concentration of the feed at constant flowrate (Figs. A5 and A7) or the feed flowrate at constant NaCl concentration (Fig. A6).

Fig. A5 shows that the more the feed saline water is loaded with salt, the more the NaCl rejection ratio decreases but remains at a very high value, close to 0.98 which will be therefore retained later.

Figs. A6 and A7 show that an increase in the feed saline water flowrate leads to a reduction in the membrane fouling induced by the concentration polarization (yellow curve and green straight line on the left of Fig. A6); but at the cost of a reduction in the water recovery rate (yellow curve and green straight line on the right of Fig. A6). This is all the more observed so as the feed saline water is loaded with salt (curves red, yellow and purple, Fig. A7). Indeed, for a given *TMP*, if we consider the permeate volumetric flux (Fig. A6), the green straight line at high feed flowrate is well above the yellow curve at lower feed flowrate; a situation which is reversed if we consider the water recovery ratio (Fig. A6); and for the same feed flowrate as the yellow curve, the purple curve of higher salt concentration is well below (Fig. A7). Regarding Fig. A7, at constant feed flowrate, the water recovery ratio decreases when the feed saline water is more and more loaded with salt, in accordance with the decrease in the permeate volumetric flux observed on Fig. A3 (which is not surprising because the two Figs. A3 and A7 are homothetic).

Typical values of *TMP* for membrane desalination process of seawater are on average 65 bar [27], a value much higher than the osmotic pressure of 25 bar previously found (for seawater at 30 g/L NaCl and 25 °C, section A1).

Consequently, by extrapolation of the water recovery ratio measured at 25 °C, in pressure up to 65 bar, then in concentration up to 30 g/L, a R_cR value close to 0.5 is obtained. This result agrees with the literature [27,37] and thus will be retained for the modeling and simulation of the RO unit.

These evaluations of *TMP* and R_cR were performed by neglecting the fouling phenomenon which will need to be prevented by punctual pure water washing cycles of the RO unit.

A3. Information got from the experiments and used for the RO unit simulation

The temperature selected for operating the RO process is 25 °C with a transmembrane pressure (*TMP*) of 65 bars, a salt rejection ratio (R_jR) of 0.98, and a water recovery ratio (R_cR) of 0.5. In order to mitigate membrane fouling without stopping the plant, a punctual circulation of pure water will be

planned.

Appendix B. Mass, energy and exergy balance equations

This Appendix gives the mass, energy and exergy balance equations for each unit of the investigated solar polygeneration plant dedicated to electricity production and desalination by considering the optimal design proposed for the ORC (configuration 3).

Table B1
Exergy balance equations.

Equations	Unit	N°
$\dot{m}_{SOLAR\_1B}\cdot\overline{Ex}_{SOLAR\_1B}+\dot{m}_{RC2.1}\cdot\overline{Ex}_{RC2.1}=\dot{m}_{SOLAR\_2B}\cdot\overline{Ex}_{SOLAR\_2B}+\dot{m}_{RC2.2}\cdot\overline{Ex}_{RC2.2}+\dot{E}x_d(RC\_RE\_HEATER)$	RC_RE_HEATER	B1
$\dot{m}_{RC2}\cdot\overline{Ex}_{RC2}+\dot{m}_{RC6}\cdot\overline{Ex}_{RC6}=\dot{m}_{RC3}\cdot\overline{Ex}_{RC3}+\dot{m}_{RC7}\cdot\overline{Ex}_{RC7}+\dot{E}x_d(RC\_REGEN)$	RC_REGEN	B2
$\dot{m}_{RC3}\cdot\overline{Ex}_{RC3}+\dot{m}_{SEA\_WATER}\cdot\overline{Ex}_{SEA\_WATER}=\dot{m}_{RC4}\cdot\overline{Ex}_{RC4}+\dot{m}_{SW2}\cdot\overline{Ex}_{SW2}+\dot{E}x_d(RC\_CONDENS)$	RC_CONDENS	B3
$\dot{m}_{RC4}\cdot\overline{Ex}_{RC4}+\dot{m}_{FEED\_EFF\_1}\cdot\overline{Ex}_{FEED\_EFF\_1}=\dot{m}_{RC5}\cdot\overline{Ex}_{RC5}+\dot{m}_{PROD\_EFF\_1}\cdot\overline{Ex}_{PROD\_EFF\_1}+\dot{E}x_d(RC\_COND\_COOL)$	RC_COND_COOL	B4
$\dot{m}_{SOLAR\_1}\cdot\overline{Ex}_{SOLAR\_1}+\dot{m}_{RC7}\cdot\overline{Ex}_{RC7}=\dot{m}_{SOLAR\_2}\cdot\overline{Ex}_{SOLAR\_2}+\dot{m}_{RC1}\cdot\overline{Ex}_{RC1}+\dot{E}x_d(RC\_BOILER)$	RC_BOILER	B5
$\dot{m}_{RC1}\cdot\overline{Ex}_{RC1}=\dot{W}_{RC\_TURBINE\_1}+\dot{m}_{RC2.1}\cdot\overline{Ex}_{RC2.1}+\dot{E}x_d(RC\_TURBINE\_1)$	RC_TURBINE_1	B6
$\dot{m}_{RC2.2}\cdot\overline{Ex}_{RC2.2}=\dot{W}_{RC\_TURBINE\_2}+\dot{m}_{RC2}\cdot\overline{Ex}_{RC2}+\dot{E}x_d(RC\_TURBINE\_2)$	RC_TURBINE_2	B7
$\dot{m}_{RC5}\cdot\overline{Ex}_{RC5}+\dot{W}_{RC\_PUMP}=\dot{m}_{RC6}\cdot\overline{Ex}_{RC6}+\dot{E}x_d(RC\_PUMP)$	RC_PUMP	B8
$\dot{m}_{SW2}\cdot\overline{Ex}_{SW2}+\dot{W}_{RO\_PUMP}=\dot{m}_{SW3}\cdot\overline{Ex}_{SW3}+\dot{E}x_d(RO\_PUMP)$	RO_PUMP	B9
$\dot{m}_{BRINE\_HP}\cdot\overline{Ex}_{BRINE\_HP}=\dot{W}_{TURB\_REC\_RO}+\dot{m}_{BRINE\_ATM}\cdot\overline{Ex}_{BRINE\_ATM}+\dot{E}x_d(TURB\_REC\_RO)$	TURB_REC_RO	B10
$\dot{m}_{RO\_PERMEATE}\cdot\overline{Ex}_{RO\_PERMEATE}=\dot{m}_{DESAL\_WATER}\cdot\overline{Ex}_{DESAL\_WATER}+\dot{E}x_d(RO\_DP\_PERM)$	RO_DP_PERM	B11
$\dot{m}_{BRINE\_RECYC}\cdot\overline{Ex}_{BRINE\_RECYC}=\dot{m}_{FEED\_EFF\_1}\cdot\overline{Ex}_{FEED\_EFF\_1}+\dot{E}x_d(B\_VALVE)$	B_VALVE	B12
$\dot{m}_{SW3}\cdot\overline{Ex}_{SW3}=\dot{m}_{BRINE\_HP}\cdot\overline{Ex}_{BRINE\_HP}+\dot{m}_{RO\_PERMEATE}\cdot\overline{Ex}_{RO\_PERMEATE}+\dot{E}x_d(RO\_MEMBRANE)$	RO_MEMRANE	B13
$\dot{m}_{BRINE\_ATM}\cdot\overline{Ex}_{BRINE\_ATM}=\dot{m}_{BRINE\_RESID}\cdot\overline{Ex}_{BRINE\_RESID}+\dot{m}_{BRINE\_RECYC}\cdot\overline{Ex}_{BRINE\_RECYC}+\dot{E}x_d(B\_SPLITTER)$	B_SPLITTER	B14
$\dot{m}_{PROD\_EFF\_1}\cdot\overline{Ex}_{PROD\_EFF\_1}=\dot{m}_{D\_EFF\_1}\cdot\overline{Ex}_{D\_EFF\_1}+\dot{m}_{B\_EFF\_1}\cdot\overline{Ex}_{B\_EFF\_1}+\dot{E}x_d(SEP\_EFF\_1)$	SEP_EFF_1	B15

Table B2
Mass and energy balance equations.

Mass balance equations (a)	Energy balance equations (b)	Unit	N°
$\dot{m}_{SOLAR\_1B}+\dot{m}_{RC2.1}=\dot{m}_{SOLAR\_2B}+\dot{m}_{RC2.2}$	$\dot{m}_{SOLAR\_1B}\cdot\overline{H}_{SOLAR\_1B}+\dot{m}_{RC2.1}\cdot\overline{H}_{RC2.1}=\dot{m}_{SOLAR\_2B}\cdot\overline{H}_{SOLAR\_2B}+\dot{m}_{RC2.2}\cdot\overline{H}_{RC2.2}$	RC_RE_HEATER	B16
$\dot{m}_{RC2}+\dot{m}_{RC6}=\dot{m}_{RC3}+\dot{m}_{RC7}$	$\dot{m}_{RC2}\cdot\overline{H}_{RC2}+\dot{m}_{RC6}\cdot\overline{H}_{RC6}=\dot{m}_{RC3}\cdot\overline{H}_{RC3}+\dot{m}_{RC7}\cdot\overline{H}_{RC7}$	RC_REGEN	B17
$\dot{m}_{RC3}+\dot{m}_{SEA\_WATER}=\dot{m}_{RC4}+\dot{m}_{SW2}$	$\dot{m}_{RC3}\cdot\overline{H}_{RC3}+\dot{m}_{SEA\_WATER}\cdot\overline{H}_{SEA\_WATER}=\dot{m}_{RC4}\cdot\overline{H}_{RC4}+\dot{m}_{SW2}\cdot\overline{H}_{SW2}$	RC_CONDENS	B18
$\dot{m}_{RC4}+\dot{m}_{FEED\_EFF\_1}=\dot{m}_{RC5}+\dot{m}_{PROD\_EFF\_1}$	$\dot{m}_{RC4}\cdot\overline{H}_{RC4}+\dot{m}_{FEED\_EFF\_1}\cdot\overline{H}_{FEED\_EFF\_1}=\dot{m}_{RC5}\cdot\overline{H}_{RC5}+\dot{m}_{PROD\_EFF\_1}\cdot\overline{H}_{PROD\_EFF\_1}$	RC_COND_COOL	B19
$\dot{m}_{SOLAR\_1}+\dot{m}_{RC7}=\dot{m}_{SOLAR\_2}+\dot{m}_{RC1}$	$\dot{m}_{SOLAR\_1}\cdot\overline{H}_{SOLAR\_1}+\dot{m}_{RC7}\cdot\overline{H}_{RC7}=\dot{m}_{SOLAR\_2}\cdot\overline{H}_{SOLAR\_2}+\dot{m}_{RC1}\cdot\overline{H}_{RC1}$	RC_BOILER	B20
$\dot{m}_{RC1}=\dot{m}_{RC2.1}$	$\dot{m}_{RC1}\cdot\overline{H}_{RC1}=\dot{W}_{RC\_TURBINE\_1}+\dot{m}_{RC2.1}\cdot\overline{H}_{RC2.1}$	RC_TURBINE_1	B21
$\dot{m}_{RC2.2}=\dot{m}_{RC2}$	$\dot{m}_{RC2.2}\cdot\overline{H}_{RC2.2}=\dot{W}_{RC\_TURBINE\_2}+\dot{m}_{RC2}\cdot\overline{H}_{RC2}$	RC_TURBINE_2	B22
$\dot{m}_{RC5}=\dot{m}_{RC6}$	$\dot{m}_{RC5}\cdot\overline{H}_{RC5}+\dot{W}_{RC\_PUMP}=\dot{m}_{RC6}\cdot\overline{H}_{RC6}$	RC_PUMP	B23
$\dot{m}_{SW2}=\dot{m}_{SW3}$	$\dot{m}_{SW2}\cdot\overline{H}_{SW2}+\dot{W}_{RO\_PUMP}=\dot{m}_{SW3}\cdot\overline{H}_{SW3}$	RO_PUMP	B24
$\dot{m}_{BRINE\_HP}=\dot{m}_{BRINE\_ATM}$	$\dot{m}_{BRINE\_HP}\cdot\overline{H}_{BRINE\_HP}=\dot{W}_{TURB\_REC\_RO}+\dot{m}_{BRINE\_ATM}\cdot\overline{H}_{BRINE\_ATM}$	TURB_REC_RO	B25
$\dot{m}_{RO\_PERMEATE}=\dot{m}_{DESAL\_WATER}$	$\dot{m}_{RO\_PERMEATE}\cdot\overline{H}_{RO\_PERMEATE}=\dot{m}_{DESAL\_WATER}\cdot\overline{H}_{DESAL\_WATER}$	RO_DP_PERM	B26
$\dot{m}_{BRINE\_RECYC}=\dot{m}_{FEED\_EFF\_1}$	$\dot{m}_{BRINE\_RECYC}\cdot\overline{H}_{BRINE\_RECYC}=\dot{m}_{FEED\_EFF\_1}\cdot\overline{H}_{FEED\_EFF\_1}$	B_VALVE	B27
$\dot{m}_{SW3}=\dot{m}_{BRINE\_HP}+\dot{m}_{RO\_PERMEATE}$	$\dot{m}_{SW3}\cdot\overline{H}_{SW3}=\dot{m}_{BRINE\_HP}\cdot\overline{H}_{BRINE\_HP}+\dot{m}_{RO\_PERMEATE}\cdot\overline{H}_{RO\_PERMEATE}$	RO_MEMRANE	B28
$\dot{m}_{BRINE\_ATM}=\dot{m}_{BRINE\_RESID}+\dot{m}_{BRINE\_RECYC}$	$\dot{m}_{BRINE\_ATM}\cdot\overline{H}_{BRINE\_ATM}=\dot{m}_{BRINE\_RESID}\cdot\overline{H}_{BRINE\_RESID}+\dot{m}_{BRINE\_RECYC}\cdot\overline{H}_{BRINE\_RECYC}$	B_SPLITTER	B29
$\dot{m}_{PROD\_EFF\_1}=\dot{m}_{D\_EFF\_1}+\dot{m}_{B\_EFF\_1}$	$\dot{m}_{PROD\_EFF\_1}\cdot\overline{H}_{PROD\_EFF\_1}=\dot{m}_{D\_EFF\_1}\cdot\overline{H}_{D\_EFF\_1}+\dot{m}_{B\_EFF\_1}\cdot\overline{H}_{B\_EFF\_1}$	SEP_EFF_1	B30

Appendix C. Detailed simulation results of the solar polygeneration plant for the various ORC designs assessed

This Appendix gives the detailed simulation results of the solar polygeneration plant for the three ORC configurations evaluated by considering as working fluid either ethyl butanoate (EB) or isopentane (IP). The streams are referred according to Figs. 3, 5, and 6 showing the ORC configurations 1, 2, and 3, respectively.

C1. Base ORC (configuration 1)

C2. ORC with a regenerator (configuration 2)

C3. ORC with a regenerator and a double-stage turbine (configuration 3)

Table C1a
Working fluid (EB or IP) streams for the base ORC (configuration 1).

Stream description	Unit	Working fluid					Working fluid				
		EB					IP				
		Stream Name					Stream Name				
		RC1	RC2	RC4	RC5	RC6	RC1	RC2	RC4	RC5	RC6
Phase		Vapor	Vapor	Vapor	Liquid	Liquid	Vapor	Vapor	Vapor	Liquid	Liquid
Temperature	°C	285.55	179.97	131.69	65.82	66.67	179.24	96.20	69.22	45.51	47.28
Pressure	bar	25.00	0.20	0.20	0.20	25.00	30.00	2.20	2.20	2.20	30.00
Molar composition											
Working fluid		1.000	1.000	1.000	1.000	1.000	1.000	1.000	1.000	1.000	1.000
Vapor mole fraction		1.0	1.0	1.0	0.0	0.0	1.0	1.0	1.0	0.0	0.0
Mass flowrate	kg/s	286.98	286.98	286.98	286.98	286.98	474.18	474.18	474.18	474.18	474.18
Mass enthalpy	kJ/kg	814.49	678.64	591.15	151.32	155.03	616.63	530.80	477.85	105.00	110.85
Mass entropy	kJ/(kg·K)	9.18631	9.21992	9.01590	7.76589	7.76746	7.78932	7.81531	7.66649	6.52339	6.52780

Table C1b
Heat transfer fluid (Therminol VP-1) streams for the base ORC (configuration 1).

Stream description	Unit	Working fluid		Working fluid	
		EB		IP	
		Stream name		Stream name	
		SOLAR_1	SOLAR_2	SOLAR_1	SOLAR_2
Phase		Vapor	Vapor	Liquid	Liquid
Temperature	°C	330.00	259.96	220.00	131.82
Pressure	bar	1.00	1.00	1.00	1.00
Molar composition					
Diphenyl oxide		0.735	0.735	0.735	0.735
Biphenyl		0.265	0.265	0.265	0.265
Vapor mole fraction		0.0	0.0	0.0	0.0
Mass flowrate	kg/s	1440.0	1440.0	1440.0	1440.0
Mass enthalpy	kJ/kg	904.70	773.28	397.17	230.62
Mass entropy	kJ/(kg·K)	6.99560	6.76417	6.04940	5.67824

Table C1c
Seawater related streams for the base ORC (configuration 1). Results are given for a vaporized mole fraction of 0.8 in the feed of the LTMED (1^{rst} effect) and in parenthesis for a vaporized mole fraction of 0.3.

Stream description	Unit	Stream name (identical results whatever the working fluid, EB or IP)					
		SEA_WATER	SW2	SW3	BRINE_HP	BRINE_ATM	DESAL_WATER
Phase		Liquid	Liquid	Liquid	Liquid	Liquid	Liquid
Temperature	°C	15.00	25.00	25.51	25.51	25.42	26.91
Pressure	bar	1.00	1.00	64.80	64.80	1.00	1.00
Molar composition							
Water		1.000	1.000	1.000	1.000	1.000	1.000
Vapor mole fraction		0.0	0.0	0.0	0.0	0.0	0.0
Mass flowrate	kg/s	600	600	600	300	300	300
Mass enthalpy	kJ/kg	63.077	104.93	112.93	112.93	106.67	112.93
Mass entropy	kJ/(kg·K)	0.22445	0.36723	0.37262	0.37262	0.37305	0.39397

Stream Description	Unit	Working fluid						Working fluid					
		EB						IP					
		Stream name						Stream name					
		BRINE_RESID	BRINE_RECYC	FEED_EFF_1	PROD_EFF_1	D_EFF_1	B_EFF_1	BRINE_RESID	BRINE_RECYC	FEED_EFF_1	PROD_EFF_1	D_EFF_1	B_EFF_1
Phase		Liquid	Liquid	Liquid	Mixed	Vapor	Liquid	Liquid	Liquid	Liquid	Mixed	Vapor	Liquid
Temperature	°C	25.42 (idem)	25.42 (idem)	25.43 (idem)	64.96 (idem)	64.96 (idem)	64.96 (idem)	25.42 (idem)	25.42 (idem)	25.44 (idem)	45.81 (idem)	45.81 (idem)	45.81 (idem)
Pressure	bar	1.00 (idem)	1.00 (idem)	0.25 (idem)	0.25 (idem)	0.25 (idem)	0.25 (idem)	1.00 (idem)	1.00 (idem)	0.10 (idem)	0.10 (idem)	0.10 (idem)	0.10 (idem)
Molar composition													
Water		1.000	1.000	1.000	1.000	1.000	1.000	1.000	1.000	1.000	1.000	1.000	1.000
Vapor mole fraction		0.0 (idem)	0.0 (idem)	0.0 (idem)	**0.8 (0.3)**	1.0 (idem)	0.0 (idem)	0.0 (idem)	0.0 (idem)	0.0 (idem)	**0.8 (0.3)**	1.0 (idem)	0.0 (idem)
Mass flowrate	kg/s	238.18 (154.74)	61.823 (145.27)	61.823 (145.27)	61.823 (145.27)	49.458 (43.579)	12.365 (101.69)	211.55 (79.765)	88.452 (220.24)	88.452 (220.24)	88.452 (220.24)	70.762 (66.071)	17.690 (154.17)
Mass enthalpy	kJ/kg	106.67 (idem)	106.67 (idem)	106.67 (idem)	2148.33 (975.58)	2617.43 (idem)	271.92 (idem)	106.66 (idem)	106.66 (idem)	106.66 (idem)	2105.46 (909.43)	2583.87 (idem)	191.81 (idem)
Mass entropy	kJ/(kg·K)	0.37305 (idem)	0.37305 (idem)	0.37335 (idem)	6.44271 (2.97420)	7.83012 (idem)	0.89308 (idem)	0.37305 (idem)	0.37305 (idem)	0.37335 (idem)	6.64892 (2.8991)	8.14885 (idem)	0.64921 (idem)

Table C2a
Working fluid (EB or IP) streams for the ORC with a regenerator (configuration 2).

Stream description	Unit	Working fluid							Working fluid						
		EB							IP						
		Stream Name							Stream Name						
		RC1	RC2	RC3	RC4	RC5	RC6	RC7	RC1	RC2	RC3	RC4	RC5	RC6	RC7
Phase		Vapor	Vapor	Vapor	Mixed	Liquid	Liquid	Liquid	Vapor	Vapor	Vapor	Mixed	Liquid	Liquid	Liquid
Temperature	°C	285.55	179.97	72.82	72.82	65.82	66.67	152.59	179.24	96.20	52.51	52.51	45.51	47.28	81.42
Pressure	bar	25.00	0.20	0.20	0.20	0.20	25.00	25.00	30.00	2.20	2.20	2.20	2.20	30.00	30.00
Molar composition															
Working fluid		1.000	1.000	1.000	1.000	1.000	1.000	1.000	1.000	1.000	1.000	1.000	1.000	1.000	1.000
Vapor mole fraction		1.000	1.000	1.000	0.735	0.000	0.000	0.000	1.000	1.000	1.000	0.837	0.000	0.000	0.000
Mass flowrate	kg/s	286.98	286.98	286.98	286.98	286.98	286.98	286.98	474.18	474.18	474.18	474.18	474.18	474.18	474.18
Mass enthalpy	kJ/kg	814.49	678.64	495.06	407.56	151.32	155.03	338.62	616.63	530.80	446.75	393.80	105.00	110.85	194.90
Mass entropy	kJ/(kg·K)	9.18631	9.21992	8.75984	8.50694	7.76589	7.76746	8.24756	7.78932	7.81531	7.57338	7.41077	6.52339	6.52780	6.77684

Table C2b
Heat transfer fluid (Therminol VP-1) streams for the ORC with a regenerator (configuration 2).

Stream description	Unit	Working fluid		Working fluid	
		EB		IP	
		Stream name		Stream name	
		SOLAR_1	SOLAR_2	SOLAR_1	SOLAR_2
Phase		Vapor	Vapor	Liquid	Liquid
Temperature	°C	330.00	280.06	220.00	147.452
Pressure	bar	1.00	1.00	1.00	1.00
Molar composition					
Diphenyl oxide		0.735	0.735	0.735	0.735
Biphenyl		0.265	0.265	0.265	0.265
Vapor mole fraction		0.0	0.0	1.0	1.0
Mass flowrate	kg/s	1440.0	1440.0	1440.0	1440.0
Mass enthalpy	kJ/kg	904.70	809.87	397.17	258.30
Mass entropy	kJ/(kg·K)	6.99560	6.83153	6.04940	5.74529

Table C2c
Seawater related streams for the ORC with a regenerator (configuration 2). Results are given for a vaporized mole fraction of 0.8 in the feed of the LTMED (1^{rst} effect) and in parenthesis for a vaporized mole fraction of 0.3. For the streams SEA_WATER, SW2, SW3, BRINE_HP, BRINE_ATM, and DESAL_WATER, please refer to Table C1b as the simulation results are identical to those obtained for the basic ORC (configuration 1). Regarding the other streams, only their flowrates change with respect to configuration 1; however, the full results were given here for reasons of clarity and consistency.

Stream Description	Unit	Working fluid						Working fluid					
		EB						IP					
		Stream name						Stream name					
		BRINE_RESID	BRINE_RECYC	FEED_EFF_1	PROD_EFF_1	D_EFF_1	B_EFF_1	BRINE_RESID	BRINE_RECYC	FEED_EFF_1	PROD_EFF_1	D_EFF_1	B_EFF_1
Phase		Liquid	Liquid	Liquid	Mixed	Vapor	Liquid	Liquid	Liquid	Liquid	Mixed	Vapor	Liquid
Temperature	°C	25.42 (idem)	25.42 (idem)	25.43 (idem)	64.96 (idem)	64.96 (idem)	64.96 (idem)	25.42 (idem)	25.42 (idem)	25.44 (idem)	45.81 (idem)	45.81 (idem)	45.81 (idem)
Pressure	bar	1.00 (idem)	1.00 (idem)	0.25 (idem)	0.25 (idem)	0.25 (idem)	0.25 (idem)	1.00 (idem)	1.00 (idem)	0.10 (idem)	0.10 (idem)	0.10 (idem)	0.10 (idem)
Molar composition													
Water		1.000	1.000	1.000	1.000	1.000	1.000	1.000	1.000	1.000	1.000	1.000	1.000
Vapor mole fraction		0.0 (idem)	0.0 (idem)	0.0 (idem)	**0.8 (0.3)**	1.0 (idem)	0.0 (idem)	0.0 (idem)	0.0 (idem)	0.0 (idem)	**0.8 (0.3)**	1.0 (idem)	0.0 (idem)
Mass flowrate	kg/s	263.98 (215.37)	36.018 (84.630)	36.018 (84.630)	36.018 (84.630)	28.814 (25.389)	7.2035 (59.241)	231.49 (129.41)	68.512 (170.59)	68.512 (170.59)	68.512 (170.59)	54.810 (51.176)	13.702 (119.41)
Mass enthalpy	kJ/kg	106.66 (idem)	106.66 (idem)	106.66 (idem)	2148.33 (975.58)	2617.43 (idem)	271.92 (idem)	106.66 (idem)	106.66 (idem)	106.66 (idem)	2105.46 (909.43)	2583.87 (idem)	191.81 (idem)
Mass entropy	kJ/(kg·K)	0.37305 (idem)	0.37305 (idem)	0.37330 (idem)	6.44271 (2.97420)	7.83012 (idem)	0.89308 (idem)	0.37305 (idem)	0.37305 (idem)	0.37335 (idem)	6.64892 (2.8991)	8.14885 (idem)	0.64921 (idem)

Table C3a
Working fluid (EB or IP) streams for the ORC with a regenerator and a double-stage turbine (configuration 3).

Stream description	Unit	Working fluid									Working fluid								
		EB									IP								
		Stream Name									Stream Name								
		RC1	RC2.1	RC2.2	RC2	RC3	RC4	RC5	RC6	RC7	RC1	RC2.1	RC2.2	RC2	RC3	RC4	RC5	RC6	RC7
Phase		Vapor	Vapor	Vapor	Vapor	Vapor	Mixed	Liquid	Liquid	Liquid	Vapor	Vapor	Vapor	Vapor	Vapor	Mixed	Liquid	Liquid	Liquid
Temperature	°C	285.55	219.03	285.55	244.89	72.82	72.82	65.82	66.67	205.00	179.24	126.06	179.24	150.09	52.51	52.51	45.51	47.28	123.09
Pressure	bar	25.00	2.24	2.24	0.20	0.20	0.20	0.20	25.00	25.00	30.00	8.10	8.10	2.20	2.20	2.20	2.20	30.00	30.00
Molar composition																			
Working fluid		1.000	1.000	1.000	1.000	1.000	1.000	1.000	1.000	1.000	1.000	1.000	1.000	1.000	1.000	1.000	1.000	1.000	1.000
Vapor mole fraction		1.000	1.000	1.000	1.000	1.000	0.712	0.000	0.000	0.000	1.000	1.000	1.000	1.000	1.000	0.819	0.000	0.000	0.000
Mass flowrate	kg/s	286.98	264.59	264.59	264.59	264.59	264.59	264.59	264.59	264.59	474.18	427.33	427.33	427.33	427.33	427.33	427.33	427.33	427.33
Mass enthalpy	kJ/kg	814.49	749.76	889.44	807.14	495.06	400.16	151.32	155.03	467.12	616.63	577.38	701.58	646.24	446.75	387.99	105.00	110.85	310.34
Mass entropy	kJ/(kg·K)	9.18631	9.20098	9.46695	9.48468	8.75984	8.48553	7.76589	7.76746	8.53189	7.78932	7.80027	8.09211	8.10669	7.57338	7.39294	6.52339	6.52780	7.08426

Table C3b
Heat transfer fluid (Therminol VP-1) streams for the ORC with a regenerator and a double-stage turbine (configuration 3).

Stream description	Unit	Working fluid				Working fluid			
		EB				IP			
		Stream name				Stream name			
		SOLAR_1	SOLAR_2	SOLAR_1B	SOLAR_2B	SOLAR_1	SOLAR_2	SOLAR_1B	SOLAR_2B
Phase		Vapor	Vapor	Vapor	Vapor	Liquid	Liquid	Liquid	Liquid
Temperature	°C	330.00	296.71	330.00	316.76	220.00	173.53	220.00	201.57
Pressure	bar	1.00	1.00	1.00	1.00	1.00	1.00	1.00	1.00
Molar composition									
Diphenyl oxide		0.735	0.735	0.735	0.735	0.735	0.735	0.735	0.735
Biphenyl		0.265	0.265	0.265	0.265	0.265	0.265	0.265	0.265
Vapor mole fraction		1.0	1.0	1.0	1.0	0.0	0.0	0.0	0.0
Mass flowrate	kg/s	1440.0	1440.0	1440.0	1440.0	1440.0	1440.0	1440.0	1440.0
Mass enthalpy	kJ/kg	904.70	840.88	904.70	879.04	397.17	306.27	397.17	360.31
Mass entropy	kJ/(kg·K)	6.99560	6.88676	6.99560	6.95257	6.04940	5.85593	6.04940	5.97323

Table C3c
Seawater related streams for the ORC with a regenerator and a double-stage turbine (configuration 3). Results are given for a vaporized mole fraction of 0.8 in the feed of the LTMED (1^{rst} effect) and in parenthesis for a vaporized mole fraction of 0.3. For the streams SEA_WATER, SW2, SW3, BRINE_HP, BRINE_ATM, and DESAL_-WATER, please refer to Table C1b as the simulation results are identical to those obtained for the basic ORC (configuration 1); so, for these streams, same results are obtained for the three configurations. Regarding the other streams, only their flowrates change with respect to configuration 1 (so, with respect to configurations 1, 2 and 3, only the flowrates change); however, the full results were given here for reasons of clarity and consistency.

Stream Description	Unit	Working fluid						Working fluid					
		EB						IP					
		Stream name						Stream name					
		BRINE_RESID	BRINE_RECYC	FEED_EFF_1	PROD_EFF_1	D_EFF_1	B_EFF_1	BRINE_RESID	BRINE_RECYC	FEED_EFF_1	PROD_EFF_1	D_EFF_1	B_EFF_1
Phase		Liquid	Liquid	Liquid	Mixed	Vapor	Liquid	Liquid	Liquid	Liquid	Mixed	Vapor	Liquid
Temperature	°C	25.42	25.42	25.43	64.96	64.96	64.96	25.42	25.42	25.44	45.81	45.81	45.81
		(idem)	(idem)	(idem)	(idem)	(idem)	(idem)	(idem)	(idem)	(idem)	(idem)	(idem)	(idem)
Pressure	bar	1.00	1.00	0.25	0.25	0.25	0.25	1.00	1.00	0.10	0.10	0.10	0.10
		(idem)	(idem)	(idem)	(idem)	(idem)	(idem)	(idem)	(idem)	(idem)	(idem)	(idem)	(idem)
Molar composition													
Water		1.000	1.000	1.000	1.000	1.000	1.000	1.000	1.000	1.000	1.000	1.000	1.000
Vapor mole fraction		0.0	0.0	0.0	**0.8**	1.0	0.0	0.0	0.0	0.0	**0.8**	1.0	0.0
		(idem)	(idem)	(idem)	**(0.3)**	(idem)	(idem)	(idem)	(idem)	(idem)	**(0.3)**	(idem)	(idem)
Mass flowrate	kg/s	267.75	32.247	32.247	32.247	25.798	6.4495	239.50	60.502	60.502	60.502	48.402	12.100
		(224.23)	(75.771)	(75.771)	(75.771)	(22.731)	(53.040)	(149.36)	(150.64)	(150.64)	(150.64)	(45.193)	(105.45)
Mass enthalpy	kJ/kg	106.66	106.66	106.66	2148.33	2617.43	271.92	106.66	106.66	106.66	2105.46	2583.87	191.81
		(idem)	(idem)	(idem)	(975.58)	(idem)	(idem)	(idem)	(idem)	(idem)	(909.43)	(idem)	(idem)
Mass entropy	kJ/(kg·K)	0.37305	0.37305	0.37330	6.44271	7.83012	0.89308	0.37305	0.37305	0.37335	6.64892	8.14885	0.64921
		(idem)	(idem)	(idem)	(2.97420)	(idem)	(idem)	(idem)	(idem)	(idem)	(2.8991)	(idem)	(idem)

Appendix D. Analysis of the heat exchangers present in the ORC of the solar polygeneration plant

This Appendix depicts the temperature profiles of the heat exchangers present in the ORC of the solar polygeneration plant investigated. The descriptions are given for the three configurations analyzed for the ORC and for each working fluid tested, i.e. ethyl butanoate (EB) and isopentane (IP). The heat transfer fluid (HTF) flowing through the solar concentrating power system, the seawater (SW), and the brine from the reverse osmosis process take also part. The heat exchangers are referred according to Figs. 3, 5, and 6 showing the ORC configurations 1, 2, and 3, respectively.

As it can be observed in the following Figs. D1-D3, there is no cross-over of temperature profiles in the heat exchangers that would lead to an inversion of the heat transfer between the hot-side stream and the cold-side stream. Furthermore, the pinch temperature difference in the heat exchangers, with state change inside at least one of the two streams, is always superior or equal to 5 °C (as adopted in the literature for evaporator and condenser in ORCs, [44]).

D1. Configuration 1 of the ORC

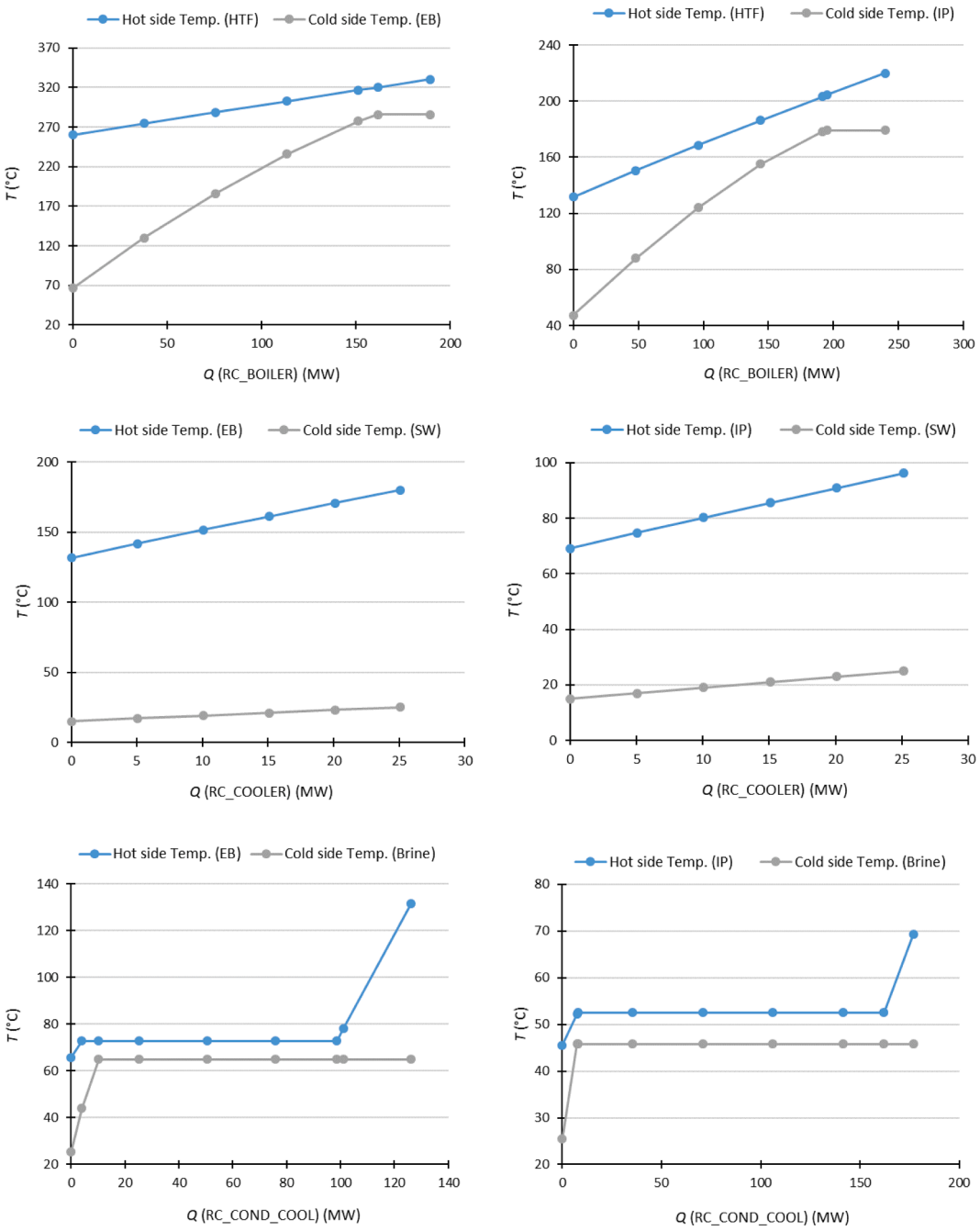

Fig. D1. Thermal profiles of the heat exchangers present in the ORC configuration 1 (base case); working fluid: ethyl butanoate (EB) on the left, isopentane (IP) on the right.

D2. Configuration 2 of the ORC

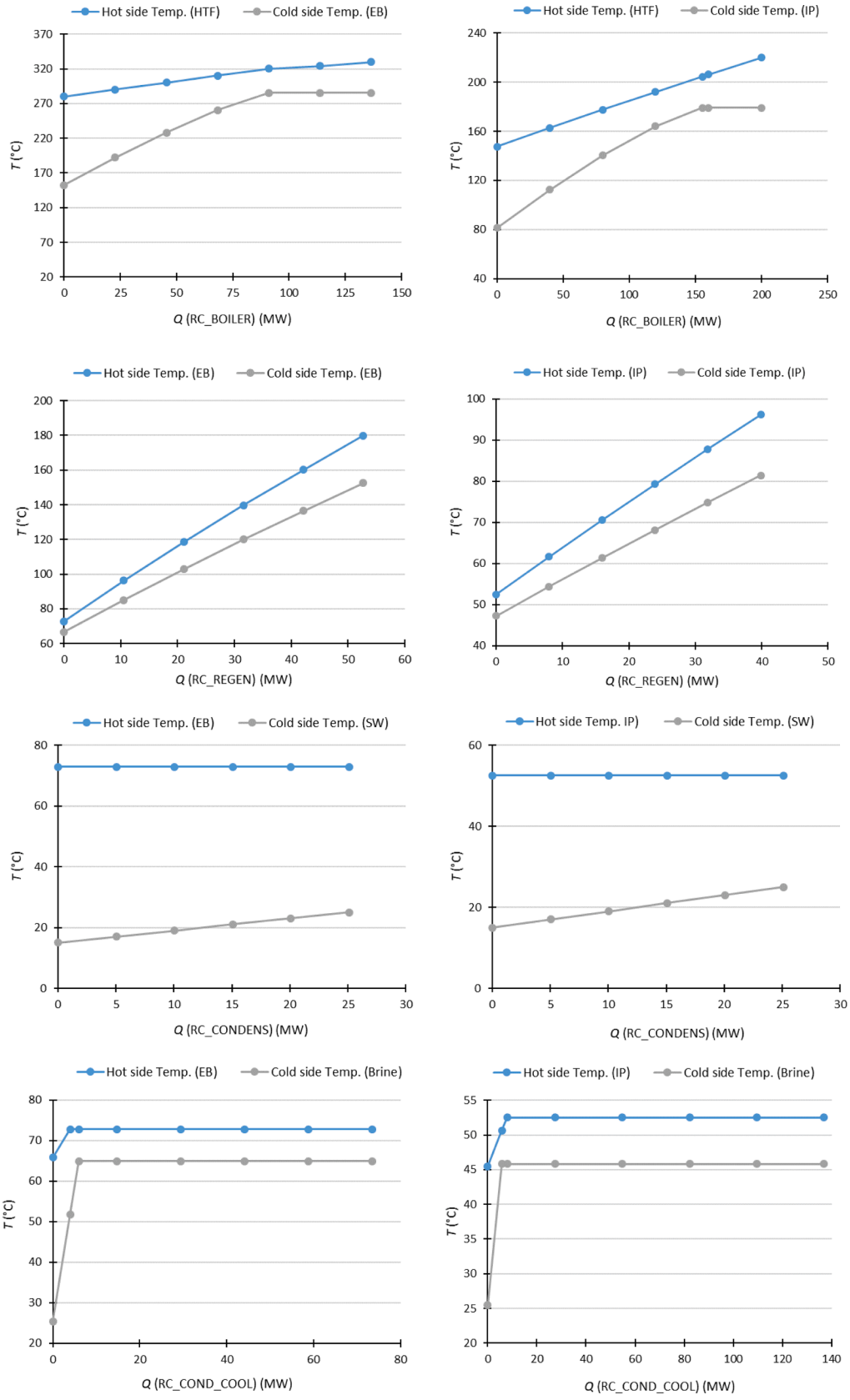

Fig. D2. Thermal profiles of the heat exchangers present in the ORC configuration 2; working fluid: ethyl butanoate (EB) on the left, isopentane (IP) on the right. Regarding the regenerator unit (RC_REGEN), the duty reported on *x*-axis is the heat rate mutually exchanged from one side to the other of the heat exchanger; the regenerator is globally adiabatic and thus $\dot{Q}$ (RC_REGEN) = 0.

D3. Configuration 3 of the ORC

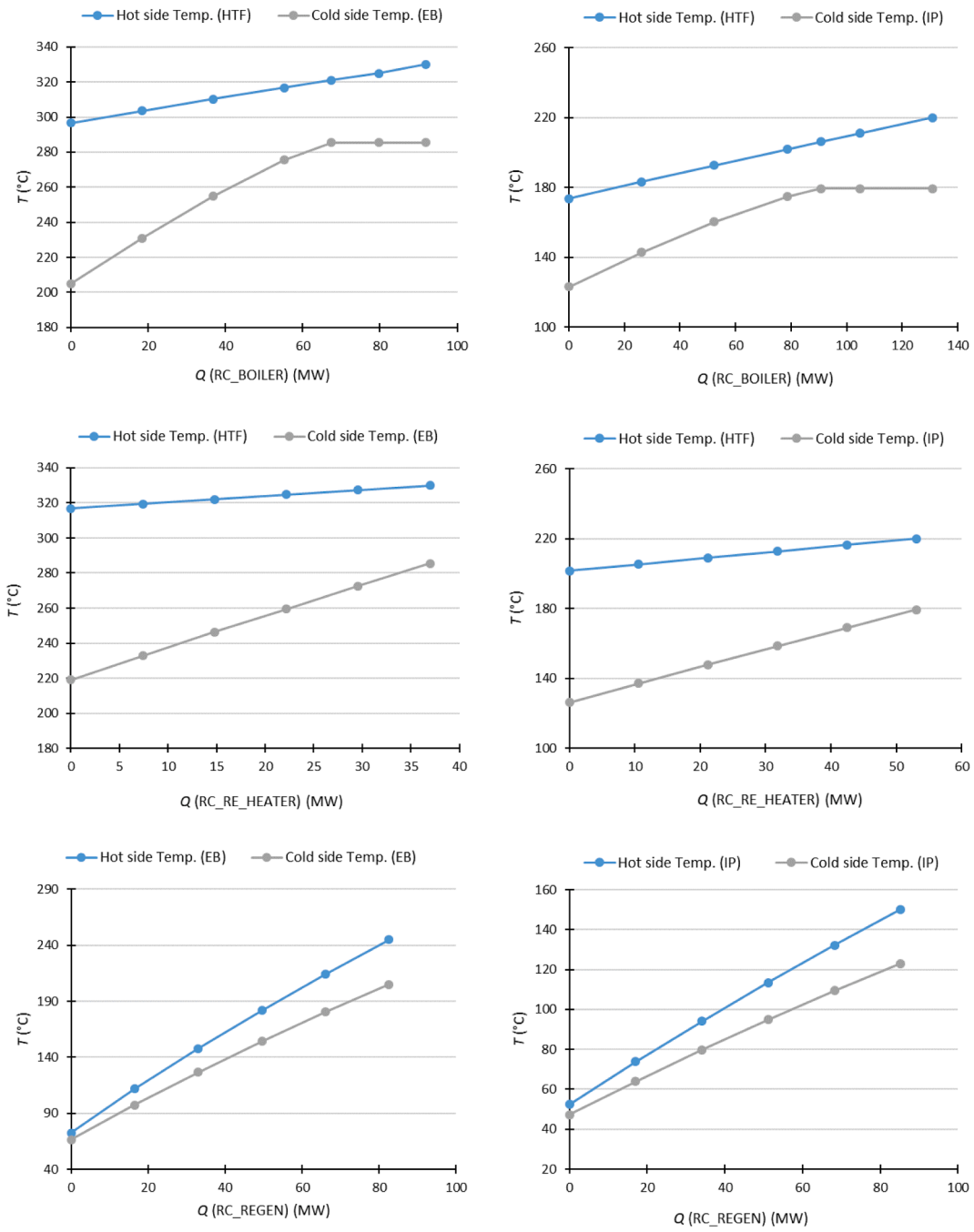

Fig. D3. Thermal profiles of the heat exchangers present in the ORC configuration 3; working fluid: ethyl butanoate (EB) on the left, isopentane (IP) on the right. Regarding the regenerator unit (RC_REGEN), the duty reported on *x*-axis is the heat rate mutually exchanged from one side to the other of the heat exchanger; the regenerator is globally adiabatic and thus $\dot{Q}$ (RC_REGEN) = 0.

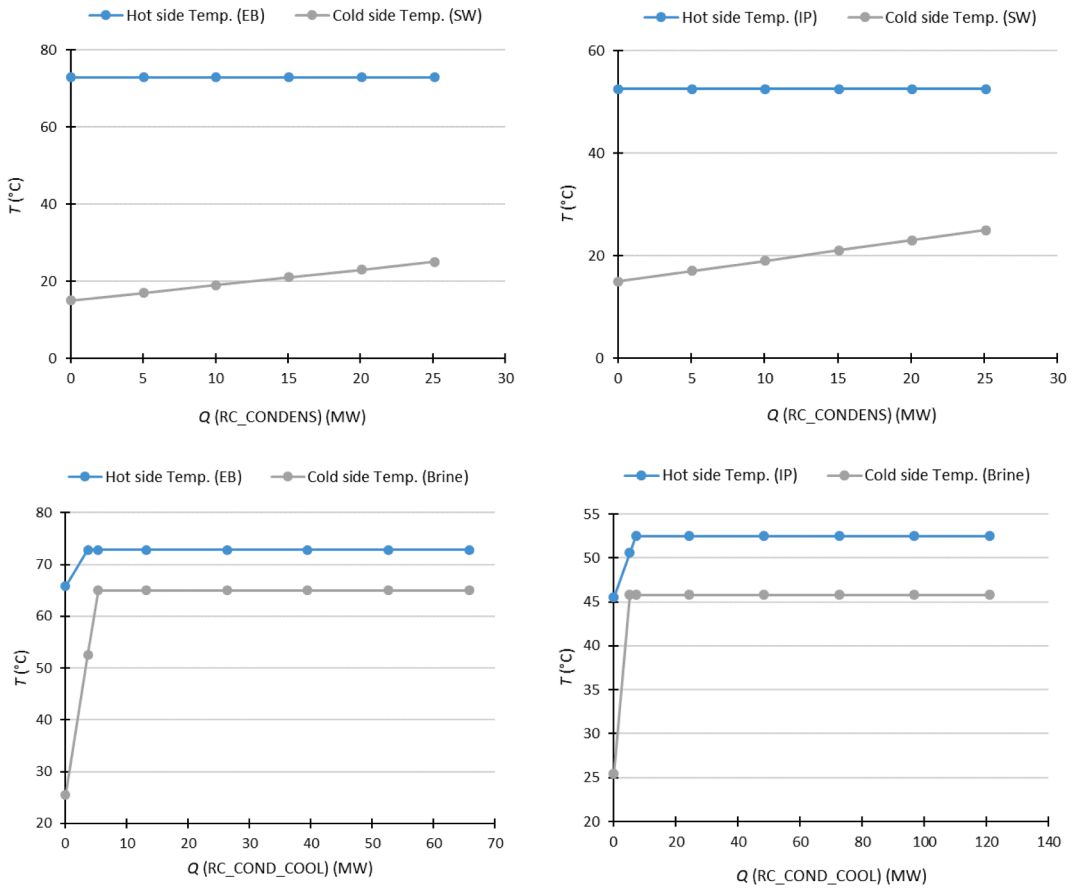

Fig. D3. (*continued*).

Appendix E. Detailed results of the economic analysis for the various ORC designs investigated

Table E1 gives the detailed results of the economic analysis performed with the Pre-Estime factor method [49] for the various ORC configurations investigated with the two working fluids, ethyl butanoate (EB) and isopentane (IP). The units are referred according to Figs. 3, 5, and 6 showing the ORC configurations 1, 2, and 3, respectively.

Table E1
Detailed results of the economic analysis performed with the Pre-Estime factor method [49] for the various ORC configurations investigated with the two working fluids, ethyl butanoate (EB) and isopentane (IP) (see Figs. 3, 5, and 6 for the unit names).

Configuration	1	2	3	1	2	3
Working fluid	EB	EB	EB	IP	IP	IP
Mass flow rate (kg/s)	286.98	286.98	264.59	474.18	474.18	427.33
Working fluid density (kg/m^3)	879	879	879	616	616	616
•RC_TURBINE (installation factor = 1.4)						
Mechanical Power (MW)	38.98	38.98	–	40.69	40.69	–
Installed price (€ 2019)	**29,748,793**	**29,748,793**	**–**	**30,833,071**	**30,833,071**	**–**
•RC_COOLER then RC_CONDENS (installation factor = 3.22)						
Thermal power (MW)	25.11	25.11	25.11	25.11	25.11	25.11
Overall heat transfer coefficient (W/m^2/K)	30	650	650	30	650	650
Average logarithmic temperature difference (K)	135	53	53	62	33	33
Exchange surface (m^2)	619	73	73	1348	118	118
Installed price (€ 2019)	**517,426**	**96,490**	**96,490**	**1,187,018**	**131,712**	**131,712**
•RC_PUMP (installation factor = 2.97)						
Mechanical Power (MW)	1.06	1.06	0.98	2.77	2.77	2.5
Volume flowrate (m3/h)	1175	1175	1084	2771	2771	2497
Installed price (€ 2019)	**1,495,815**	**1,495,815**	**1,387,117**	**3,371,481**	**3,371,481**	**3,053,484**
•RC_COND_COOL (installation factor = 3.22)						
Thermal power (MW)	126.22	73.54	65.84	176.8	136.94	120.93
Overall heat transfer coefficient (W/m^2/K)	650	650	650	650	650	650
Average logarithmic temperature difference (K)	53	20	20	22	13	13
Exchange surface (m^2)	368	562	503	1252	1677	1481
Material factor - Vaporized mole fraction (VF) = 0.8	2.2	2.2	2.2	2.2	2.2	2.2
Material factor - Vaporized mole fraction (VF) = 0.3	1.0	1.0	1.0	1.0	1.0	1.0

(*continued on next page*)

Table E1 (*continued*)

Configuration	1	2	3	1	2	3
Working fluid	EB	EB	EB	IP	IP	IP
Mass flow rate (kg/s)	286.98	286.98	264.59	474.18	474.18	427.33
Working fluid density (kg/m^3)	879	879	879	616	616	616
Installed price - VF = 0.8 (€ 2019)	**700,870**	**1,035,426**	**932,052**	**2,399,706**	**3,383,333**	**2,915,868**
Installed price - VF = 0.3 (€ 2019)	**318,577**	**470,648**	**423,660**	**1,090,776**	**1,537,879**	**1,325,394**
•RC_BOILER (installation factor = 3.22)						
•Preheater section						
Thermal power (MW)	161.75	91.04	67.39	195.16	159.98	90.63
Overall heat transfer coefficient (W/m^2/K)	50	50	50	600	600	600
Average logarithmic temperature difference (K)	92	71	58	49	42	38
Exchange surface (m^2)	3518	2563	2306	661	628	400
Installed price preheater section (€ 2019)	4,737,471	3,078,063	2,680,933	645,698	613,195	401,270
•Evaporator section						
Thermal power (MW)	27.5	45.53	24.524	44.67	39.99	40.25
Overall heat transfer coefficient (W/m^2/K)	650	650	650	650	650	650
Average logarithmic temperature difference (K)	39	39	39	32	32	34
Exchange surface (m^2)	108	179	96	212	190	184
Installed price evaporator section (€ 2019)	145,113 €	207,539	134,500	236,319	217,047	211,824
Installed price (€ 2019)	**4,882,584**	**3,285,602**	**2,815,433**	**882,017**	**830,241**	**613,094**
•RC_REGEN (installation factor = 3.22)						
Thermal power (MW)	–	52.69	82.58	–	39.86	85.25
Overall heat transfer coefficient (W/m^2/K)	–	50	50	–	50	50
Average logarithmic temperature difference (K)	–	14	18	–	10	14
Exchange surface (m^2)	–	7547	9215	–	8116	12,212
Installed price (€ 2019)	**–**	**7,948,677**	**9,935,846**	**–**	**8,942,261**	**12,916,600**
•RC_TURBINE_1 (installation factor = 1.4)						
Mechanical Power (MW)	–	–	17.13	–	–	16.77
Installed price (€ 2019)	**–**	**–**	**14,987,265**	**–**	**–**	**14,724,173**
•RC_RE_HEATER (installation factor = 3.22)						
Thermal power (MW)	–	–	36.96	–	–	53.08
Overall heat transfer coefficient (W/m^2/K)	–	–	50	–	–	50
Average logarithmic temperature difference (K)	–	–	68	–	–	57
Exchange surface (m^2)	–	–	1091	–	–	1872
Installed price (€ 2019)	**–**	**–**	**1,093,674**	**–**	**–**	**2,059,011**
•RC_TURBINE_2 (installation factor = 1.4)						
Mechanical Power (MW)	–	–	21.78	–	–	23.65
Installed price (€ 2019)	**–**	**–**	**18,310,114**	**–**	**–**	**19,611,906**
CEPCI Index 2000	394.1	394.1	394.1	394.1	394.1	394.1
CEPCI Index 2019	607.5	607.5	607.5	607.5	607.5	607.5
TOTAL PRICE (€ 2019)	37,345,488	43,610,802	49,557,991	38,673,293	47,492,099	56,025,847
Environment factor	1.8	1.8	1.8	1.8	1.8	1.8
CAPEX (€ 2019)	**67,221,878**	**78,499,443**	**89,204,383**	**69,611,928**	**85,485,779**	**100,846,525**
Annual production time (h)	8000	8000	8000	8000	8000	8000
Net produced electrical power (MW)	37.92	37.92	37.93	37.92	37.92	37.92
Electricity cost (€/kWh)	0.05	0.05	0.05	0.05	0.05	0.05
Income from the sale of electricity (€ 2019 /year)	15,168,000	15,168,000	15,172,000	15,168,000	15,168,000	15,168,000
Payback time (year)	**4.43**	**5.18**	**5.88**	**4.59**	**5.64**	**6.65**

References

[1] H. Mokhtari, M. Sepahvand, A. Fasihfar, Thermoeconomic and exergy analysis in using hybrid systems (GT+MED+RO) for desalination of brackish water in Persian Gulf, Desalination 399 (2016) 1–15, https://doi.org/10.1016/j.desal.2016.07.044.

[2] E.A. Chadegani, M. Sharifishourabi, F. Hajiarab, Comprehensive assessment of a multi-generation system integrated with a desalination system: Modeling and analyzing, Energy Convers. Manage. 174 (2018) 20–32, https://doi.org/10.1016/j.enconman.2018.08.011.

[3] A. Kasaeian, E. Bellos, A. Shamaeizadeh, C. Tzivanidis, Solar-driven polygeneration systems: Recent progress and outlook, Appl. Energy 264 (2020), 114764, https://doi.org/10.1016/j.apenergy.2020.114764.

[4] L.M. Serra, A. LozanoM, J. Ramos, A.V. Ensinas, S.A. Nebra, Polygeneration and efficient use of natural resources, Energy 34 (2009) 575–586, https://doi.org/10.1016/j.energy.2008.08.013.

[5] A. Keshvarparast, S.S.M. Ajarostaghi, M.A. Delavar, Thermodynamic analysis the performance of hybrid solar-geothermal power plant equipped with air-cooled condenser, Appl. Therm. Eng. 172 (2020), 115160, https://doi.org/10.1016/j.applthermaleng.2020.115160.

[6] R. Maali, T. Khir, Performance analysis of different orc power plant configurations using solar and geothermal heat sources, Int. J. Green Energy 17 (2020) 349–362, https://doi.org/10.1080/15435075.2020.1731517.

[7] C. Mata-Torres, R.A. Escobar, J.M. Cardemil, Y. Simsek, J.A. Matute, Solar polygeneration for electricity production and desalination: Case studies in Venezuela and northern Chile, Renew. Energy 101 (2017) 387–398, https://doi.org/10.1016/j.renene.2016.08.068.

[8] A.M. Pantaleo, S.M. Camporeale, A. Sorrentino, A. Miliozzi, N. Shah, C. N. Markides, Hybrid solar-biomass combined Brayton/organic Rankine-cycle plants integrated with thermal storage: Techno-economic feasibility in selected Mediterranean areas, Renew. Energy 147 (2020) 2913–2931, https://doi.org/10.1016/j.renene.2018.08.022.

[9] A. Kasaeian, F. Fatemeh Rajaee, W.M. Yan, Osmotic desalination by solar energy: A critical review, Renew. Energy 134 (2019) 1473–1490, https://doi.org/10.1016/j.renene.2018.09.038.

[10] Y. Zheng, R. Caceres Gonzalez, M.C. Hatzell, K.B. Hatzell, Concentrating solar thermal desalination: Performance limitation analysis and possible pathways for improvement, Appl. Therm. Eng. 184 (2021), 116292, https://doi.org/10.1016/j.applthermaleng.2020.116292.

[11] R. Rayegan, Y.X. Tao, A procedure to select working fluids for Solar Organic Rankine Cycles (ORCs), Renew. Energy 36 (2011) 659–670, https://doi.org/10.1016/j.renene.2010.07.010.

[12] S. Quoilin, M. Orosz, H. Hemond, V. Lemort, Performance and design optimization of a low-cost solar organic Rankine cycle for remote power generation, Sol. Energy 85 (2011) 955–966, https://doi.org/10.1016/j.solener.2011.02.010.

[13] G.H. Lopes, N. Ibaseta, P. Guichardon, P. Haldenwang, Predicting Permeate Fluxes and Rejection Rates in Reverse Osmosis and Tight-Nanofiltration Processes, Chem. Eng. Technol. 38 (2015) 585–594, https://doi.org/10.1002/ceat.201400654.

[14] T.Y. Qiu, P.A. Davies, Concentration polarization model of spiral-wound membrane modules with application to batch-mode RO desalination of brackish water, Desalination 368 (2015) 36–47, https://doi.org/10.1016/j.desal.2014.12.048.

[15] A. Al-Karaghouli, L.L. Kazmerski, Energy consumption and water production cost of conventional and renewable-energy-powered desalination processes, Renew. Sustain. Energy Rev. 24 (2013) 343–356, https://doi.org/10.1016/j.rser.2012.12.064.

[16] I.B. Askari, M. Ameri, A techno-economic review of multi effect desalination systems integrated with different solar thermal sources, Appl. Therm. Eng. 185 (2021), 116323, https://doi.org/10.1016/j.applthermaleng.2020.116323.
[17] A. Panagopoulos, K.J. Haralambous, M. Loizidou, Desalination brine disposal methods and treatment technologies - A review, Sci. Total Environ. 693 (2019), 133545, https://doi.org/10.1016/j.scitotenv.2019.07.351.
[18] H. Sharon, K.S. Reddy, A review of solar energy driven desalination technologies, Renew. Sustain. Energy Rev. 41 (2015) 1080–1118, https://doi.org/10.1016/j.rser.2014.09.002.
[19] B. Ortega-Delgado, M. Cornali, P. Palenzuela, D.C. Alarcón-Padilla, Operational analysis of the coupling between a multi-effect distillation unit with thermal vapor compression and a Rankine cycle power block using variable nozzle thermocompressors, Appl. Energy 204 (2017) 690–701, https://doi.org/10.1016/j.apenergy.2017.07.062.
[20] B.F. Tchanche, G. Lambrinos, A. Frangoudakis, G. Papadakis, Low-grade heat conversion into power using organic Rankine cycles – A review of various applications, Renew. Sustain. Energy Rev. 15 (2011) 3963–3979, https://doi.org/10.1016/j.rser.2011.07.024.
[21] N. Yabuuchi, K. Kubota, M. Dahbi, S. Komaba, Research Development on Sodium-Ion Batteries, Chem. Rev. 114 (2014) 11636–11682, https://doi.org/10.1021/cr500192f.
[22] C. Fernandez-Gonzalez, A. Dominguez-Ramos, R. Ibañez, Y. Chen, A. Irabien, Valorization of desalination brines by electrodialysis with bipolar membranes using nanocomposite anion exchange membranes, Desalination 406 (2017) 16–24, https://doi.org/10.1016/j.desal.2016.07.033.
[23] M. Herrero-Gonzalez, P. Diaz-Guridi, A. Dominguez-Ramos, A. Irabien, R. Ibañez, Highly concentrated HCl and NaOH from brines using electrodialysis with bipolar membranes, Sep. Purif. Technol. 242 (2020), 116785, https://doi.org/10.1016/j.seppur.2020.116785.
[24] B. Anand, R. Shankar, S. Murugavelh, W. Rivera, K.M. Prasad, R. Nagarajan, A review on solar photovoltaic thermal integrated desalination technologies, Renew. Sustain. Energy Rev. 141 (2021), 110787, https://doi.org/10.1016/j.rser.2021.110787.
[25] P. Palenzuela, G. Zaragoza, D.C. Alarcón-Padilla, E. Guillén, M. Ibarra, J. Blanco, Assessment of different configurations for combined parabolic-trough (PT) solar power and desalination plants in arid regions, Energy 36 (2011) 4950–4958, https://doi.org/10.1016/j.energy.2011.05.039.
[26] P. Palenzuela, D.-C. Alarcón-Padilla, G. Zaragoza, Large-scale solar desalination by combination with CSP: Techno-economic analysis of different options for the Mediterranean Sea and the Arabian Gulf, Desalination 366 (2015) 130–138, https://doi.org/10.1016/j.desal.2014.12.037.
[27] P. Palenzuela, B. Ortega-Delgado, D.C. Alarcón-Padilla, Comparative assessment of the annual electricity and water production by concentrating solar power and desalination plants: A case study, Appl. Therm. Eng. 177 (2020), 115485, https://doi.org/10.1016/j.applthermaleng.2020.115485.
[28] J.C. Bruno, J. Lopez-Villada, E. Letelier, S. Romera, A. Coronas, Modelling and optimisation of solar organic rankine cycle engines for reverse osmosis desalination, Appl. Therm. Eng. 28 (2008) 2212–2226, https://doi.org/10.1016/j.applthermaleng.2007.12.022.
[29] D.H. Bowskill, U.E. Tropp, S. Gopinath, G. Jackson, A. Galindo, C.S. Adjiman, Beyond a heuristic analysis: integration of process and working-fluid design for organic Rankine cycles, Mol. Syst. Des. Eng. 5 (2020) 493, https://doi.org/10.1039/C9ME00089E.
[30] ProII SimSci, 2018 Schneider Electric Software, version 10.1.2.
[31] D.Y. Peng, D.B. Robinson, A new two-constant equation of state, Ind. Eng. Chem. Fundam. 15 (1976) 59–64, https://doi.org/10.1021/i160057a011.
[32] A. Pina-Martinez, Y. Le Guennec, R. Privat, J.N. Jaubert, P.M. Mathias, Analysis of the Combinations of Property Data That Are Suitable for a Safe Estimation of Consistent Twu α-Function Parameters: Updated Parameter Values for the Translated-Consistent tc-PR and tc-RK Cubic Equations of State, J. Chem. Eng. Data 63 (10) (2018) 3980–3988, https://doi.org/10.1021/acs.jced.8b00640.
[33] M.H. Sharqawy, J.H. Lienhard, S.M. Zubair, Thermophysical properties of seawater: a review of existing correlations and data, Desalin. Water Treat. 16 (2010) 354–380, https://doi.org/10.5004/dwt.2010.1079.
[34] V.S. Reddy, S.C. Kaushik, S.K. Tyagi, Exergetic analysis and performance evaluation of parabolic trough concentrating solar thermal power plant (PTCSTPP), Energy 39 (2012) 258–273, https://doi.org/10.1016/j.energy.2012.01.023.
[35] J. Bao, L. Zhao, A review of working fluid and expander selections for organic Rankine cycle, Renew. Sustain. Energy Rev. 24 (2013) 325–342, https://doi.org/10.1016/j.rser.2013.03.040.
[36] V. Papaioannou, T. Lafitte, C. Avendaño, C.S. Adjiman, G. Jackson, E.A. Müller, A. Galindo, J. Chem. Phys. 140 (2014), 054107, https://doi.org/10.1063/1.4851455.
[37] K. Rahbar, S. Mahmoud, R.K. Al-Dadah, N. Moazami, S.A. Mirhadizadeh, Review of organic Rankine cycle for small-scale applications, Energy Convers. Manage. 134 (2017) 135–155, https://doi.org/10.1016/j.enconman.2016.12.023.
[38] G. Iaquaniello, A. Salladini, A. Mari, A.A. Mabrouk, H.E.S. Fath, Concentrating solar power (CSP) system integrated with MED–RO hybrid desalination, Desalination 336 (2014) 121–128, https://doi.org/10.1016/j.desal.2013.12.030.
[39] W. Zhou, L. Song, T.K. Guan, A numerical study on concentration polarization and system performance of spiral wound RO membrane modules, J. Membr. Sci. 271 (2006) 38–46, https://doi.org/10.1016/j.memsci.2005.07.007.
[40] M.H. Khoshgoftar Manesh, H. Ghalami, M. Amidpour, M.H. Hamedi, Optimal coupling of site utility steam network with MED-RO desalination through total site analysis and exergoeconomic optimization, Desalination 316 (2013) 42–52, https://doi.org/10.1016/j.desal.2013.01.022.
[41] A. Piacentino, Application of advanced thermodynamics, thermoeconomics and exergy costing to a Multiple Effect Distillation plant: In-depth analysis of cost formation process, Desalination 371 (2015) 88–103, https://doi.org/10.1016/j.desal.2015.06.008.
[42] S. Sadri, M. Ameri, R.H. Khoshkhoo, Multi-objective optimization of MED-TVC-RO hybrid desalination system based on the irreversibility concept, Desalination 402 (2017) 97–108, https://doi.org/10.1016/j.desal.2016.09.029.
[43] R.S. El-Emam, I. Dincer, Thermodynamic and thermoeconomic analyses of seawater reverse osmosis desalination plant with energy recovery, Energy 64 (2014) 154–163, https://doi.org/10.1016/j.energy.2013.11.037.
[44] C. He, C. Liu, H. Gao, H. Xie, Y. Li, S. Wu, J. Xu, The optimal evaporation temperature and working fluids for subcritical organic Rankine cycle, Energy 38 (2012) 136–143, https://doi.org/10.1016/j.energy.2011.12.022.
[45] P. Talebbeydokhti, A. Cinocca, R. Cipollone, B. Morico, Analysis and optimization of LT-MED system powered by an innovative CSP plant, Desalination 413 (2017) 223–233, https://doi.org/10.1016/j.desal.2017.03.019.
[46] V.A.F. Costa, On the exergy balance equation and the exergy destruction, Energy 116 (2016) 824–835, https://doi.org/10.1016/j.energy.2016.10.015.
[47] N. Nazari, S. Porkhial, Multi-objective optimization and exergo-economic assessment of a solar-biomass multi-generation system based on externally-fired gas turbine, steam and organic Rankine cycle, absorption chiller and multi-effect desalination, Appl. Therm. Eng. 179 (2020), 115521, https://doi.org/10.1016/j.applthermaleng.2020.115521.
[48] Y. Kansha, N. Tsuru, K. Sato, C. Fushimi, A. Tsutsumi, Self-heat recuperation technology for energy saving in chemical processes, Ind. Eng. Chem. Res. 48 (2009) 7682–7686, https://doi.org/10.1021/ie9007419.
[49] A. Chauvel, G. Fournier, Raimbault, Technip Edition, Manual of process economic evaluation, 2004.
[50] M.Y. Ho, J. Geddes, E. Barmatov, L. Crawford, T. Hughes, Effect of composition and microstructure of duplex stainless steel on adsorption behaviour and efficiency of corrosion inhibitors in 4 molar hydrochloric acid. Part I: standard DSS 2205, Corros. Sci. 137 (2018) 43–52, https://doi.org/10.1016/j.corsci.2018.03.022.
[51] M.A. Deyab, Enhancement of corrosion resistance in MSF desalination plants during acid cleaning operation by cationic surfactant, Desalination 456 (2019) 32–37, https://doi.org/10.1016/j.desal.2019.01.018.